# GREENLAND ICE SHEET CLIMATOLOGY AND SURFACE ENERGY BALANCE MODELING:
## GREENLAND CLIMATE NETWORK (GC-NET)

**K. Steffen and J. Box, N. Cullen**
**University of Colorado at Boulder**
**Cooperative Institute for Research in Environmental Sciences**
**Division of Cryospheric and Polar Processes**
**Campus Box 216, Boulder CO 80309**

NAGW-4248
Progress Report

Request for Extension of Existing Grant
4/1/00 – 3/31/04
S 893,015

to
National Aeronautics and Space Administration
January 2000

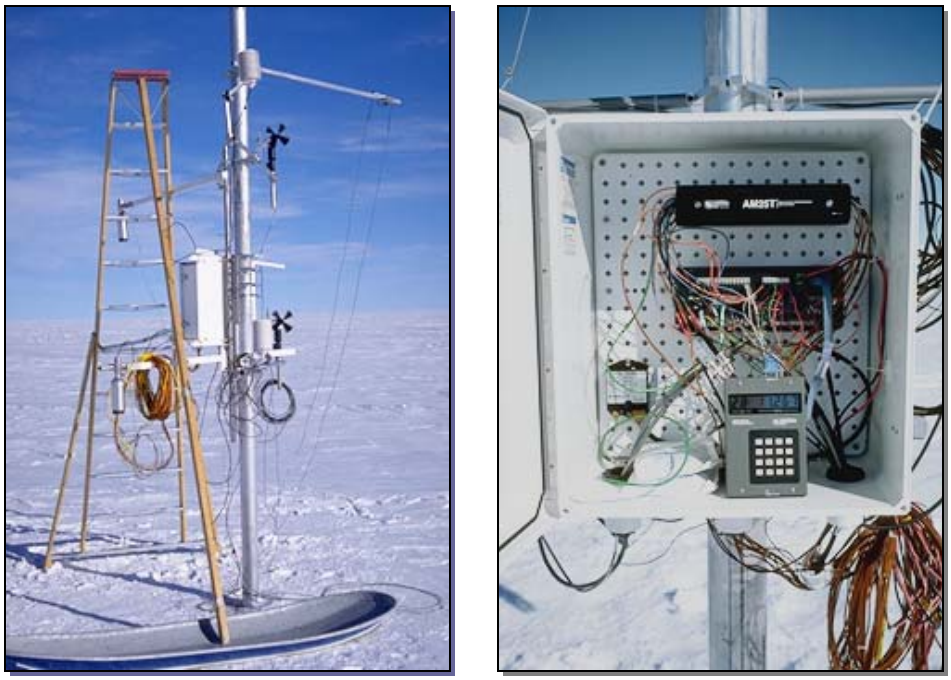

INSTALLATION OF TUNU-N AWS (LEFT), AND INSTRUMENT BOX (RIGHT)

# TABLE OF CONTENTS

# SUMMARY OF HIGHLIGHTS

## *Greenland Climate Network*

- Three new automatic weather stations (JAR2, KULU, KAR) have been installed during the '99 field season to increase the GC-Net to a total of 18 stations.
- Fourteen AWS maintenance jobs were carried out at Swiss Camp, JAR, Crawford Point-1, Crawford Point-2, Summit, DYE2, GITS, NASA-U, NASA-E, NASA-SE, S-Dome, Humboldt, TUNU-N, and Saddle.
- A complete annual GPS record was recovered from the Swiss Camp, with weekly measurements covering the time period June 98 to May 99. The Trimble 4000SSE instrument was powered by solar panels connected to four 100 Ah batteries.
- 50+ station years of GC-Net measurements have been processed and are available for the general science community.
- Measurements of relative humidity have been scaled for temperatures below 0 ºC with respect to saturation pressure over ice.

## *Greenland Ice Sheet Climatology*

- Thirteen papers have been published or are in press in peer-reviewed journals supported by this grant, and 3 more papers are ready to be submitted to a peer-reviewed journal.
- Sublimation rates for 15 AWS sites have been compiled using 5 different methods. The sublimation shows a strong seasonal cycle, ranging from 0 (in winter) to 100 W $m^{-2}$ (summer) for the latent heat flux on a monthly mean basis.
- Sublimation rates from the AWS sites have been compared with GISS-99 model output, and the results indicate that the GISS model is smaller than the GC-Net data by 40% - 100%.
- A comparison of the bulk aerodynamic and eddy correlation method to calculate the turbulent fluxes using GC-Net data showed good agreement, with a mean total error less than 8% for both methods.
- The estimates of sublimation and evaporation using the bulk aerodynamic method supports the decision to maintain a two level profile on the network of AWS over the Greenland ice sheet.
- Using a surface-fixed and towed parafoil system, a variety of measurements could be made during wind speed between 0 - 20 m $s^{-1}$. A typical wave-like activity at the top of the boundary layer was detected with a wave period of approximately 40 s.
- At the Swiss Camp a surface height change of –0.24 m per year was measured using a geodetic method (GPS instruments) for the time period 1994 to 1999. This decrease is related with the increasing surface air temperature of +0.9 ºC per year from the same location.
- The comparison of a topographical survey between 1995 and 1999 revealed a volume change of –827,374 $m^3$, which means a decreasing thickness of 0.24 m per year, which is in agreement with the geodetic method and some recent satellite and aircraft measurements.

# 1. INTRODUCTION

## *1.1 Rational of the Study*

Climatological observations and surface energy balance studies are the keys to the understanding of the surface processes linked with ice sheet mass balance. Long-term climate records at different sites on the ice sheet are needed for the assessment of the snow pack energy and mass balance of the accumulation zone and to gain more complete information of the spatial variation of climate over the ice sheet. A considerable amount of surface energy and mass balance data as well as some ice cores have been collected at the ETH/CU research camp since 1990. The camp is located at the ice sheet equilibrium line altitude (ELA), about 89 km east of Jakobshavn at 69° 34' N, 49° 17' W on the western margin of the Greenland ice sheet (Fig. 1.1). Seven years of detailed climatological and glaciological measurements at the camp provide valuable insight on the magnitude of the seasonal and interannual variability in the equilibrium zone. Based on the ETH/CU camp energy flux measurements, a simple climate sensitivity model calculation showed, that during a 3 °C temperature increase scenario, approximately 22 $km^3$ water equivalent of snow would sublimate. This equals 4% of today's annual accumulation. Large seasonal and interannual variations in air temperature and wind speed were found for the location of the ETH/CU camp based on the seven year record. Surface temperature anomalies in the order of -3° C along the west coast of Greenland for the winter months have also been reported since 1990. In contrast, a notable increasing trend of 4.5% per year in melt area has been observed between the years 1979-91, which came to an abrupt halt in 1992 after the eruption of Mt. Pinatubo. A similar trend is observed in the temperatures at six coastal stations.

The Greenland Climate Network (GC-Net) was established in spring 1994 with the emphasis to monitor climatological and glaciological parameters at various locations on the ice sheet over a time period of at least 10 years. The objectives of the GC-Net automatic weather station (AWS) network are:

- Assess daily, annual and interannual variability in accumulation rate, surface climatology and surface energy balance at selected locations on the ice sheet where high sensitivity of the ice sheet mass balance to climate anomalies is predicted from modeling results.
- Assess accurate surface elevation, location, near-surface density at the AWS location with the option to revisit the locations in order to get temporal information for dynamic ice sheet modeling.
- The objective of this study is to model the surface energy balance based on atmospheric and cyrospheric interactions, using the Greenland climate network of AWS stations as input parameters. In a first attempt, the surface energy balance of the western part of the ice sheet will be modeled, using the current AWS network.

Another important factor is the surface topography. The surface topography with scale length of several kilometers plays an important role in the spatial variability of accumulation. The knowledge of this surface roughness is essential for the spatial surface energy balance modeling. One of the major applications of ice core data is the estimation of snow accumulation in the vicinity of the core location. A major problem arises however inidentification of the date of peak isotope. A one month underestimation in one year followed by a one month overestimation in another, results in a time error of 17%. Such an error significantly alters the estimated annual accumulation rates. Using a combination of different passive microwave frequencies with their varying penetration depths, estimates of the date of maximum and minimum surface temperatures can be made as a function of the brightness temperature characteristics. These minimum temperature estimates can be correlated with air temperatures recorded by existing AWS.

## *1.2 Logistic Summary '99*

| Date | Location | Work |
|---|---|---|
| ***March 1999*** | | |
| 23-30 | Sondrestromfjord (SFJ) | Swiss Camp preparation |
| 30-31 | Swiss Camp | Camp opening, data retrieval, AWS reactivation |
| ***April 1999*** | | |
| 1-10 | Swiss Camp | 1-D Eddy correlation and ventilated temperature sensor setup<br>Install 2 new masts, test GPS on AWS, test transmission |
| 10-14 | SFJ | AWS southern traverse preparation |
| 14-17 | Saddle | AWS maintenance and extension, GPS, Snow Pit |
| 17-21 | DYE-2 Raven | AWS maintenance, GPS, 53 knot storm, Snow Pit |
| 21-22 | NASA-SE | AWS maintenance, GPS, Snow Pit |
| 22-24 | South Dome | AWS maintenance and extension, GPS, Snow Pit |
| 24-27 | SFJ | AWS northern traverse preparation |
| 27-29 | Thule | Camping re-supply |
| | GITS | AWS maintenance and extension, Snow Pit |
| ***May 1999*** | | |
| 1-4 | GITS | Transmitter trouble shooting, GPS |
| 4-6 | Humboldt | AWS maintenance, GPS, Snow Pit |
| 6 | Thule | Overnight, return northern cargo to SFJ |
| 7 | SFJ | Central, east, and north east traverse preparation |
| 8-13 | Summit (SUM) | AWS maintenance and extension, GPS, Snow Pit |
| 13 | NASA-U | AWS maintenance and extension, GPS, Snow Pit |
| 14 | NASA-U→SUM | Constable Pt. (CNP) |
| 16-18 | KAR | Kanderlussuaq accumulation region (KAR) AWS installation<br>GPS, Snow Pit |
| 18-20 | CNP | |
| 20 | NASA-E, TUNU-N | AWS maintenance |
| | CNP→SFJ | Preparation for Swiss Camp |
| 21-25 | Swiss Camp | Temperature comparison, AWS maintenance and testing. |
| 25-28 | Crawford Point 1 & 2 | Skidoo traverse, AWS maint., CP1 extension, GPS,<br>Snow Pit, Ground penetrating RADAR survey CP1 to CP2 |
| 29-31 | Swiss Camp | Eddy correlation, traverse preparation. |
| 31 | JAR | AWS maintenance, extension, GPS |
| 31 | JAR→JAR2 | JAR2 recon. by snow mobile, no need for helicopter! |
| 31-June 02 | Swiss Camp | JAR2 traverse preparation |
| ***June 1999*** | | |
| | JAR 2 | AWS installation, GPS |
| 03-08 | Swiss Camp | Temperature comparison |
| 08-09 | CP1 and CP 2 | Return by skidoo for transmitter reactivation |
| 09-16 | Swiss Camp | Construction of couloir connecting the entire camp |
| 16 | SC→JAV→SFJ | Swiss Camp pullout to SFJ |
| 16 | SFJ→Nuuk | KULU AWS preparation |
| 17 | Nuuk→Kulusuk | |
| 17-19 | Kulusuk | Preparation for KULU work |
| 19 | KULU | Install KULU AWS SE Greenland ablation zone, GPS |
| | Angmassalik | Overnight |
| | Kulusuk | Organize cargo for return to W Greenland, overnight |
| | Kulusuk→Nuuk→SFJ | Transit |
| 23 | SFJ→CONUS | Transit |

## *1.3 Personal*

| Name | Institution | Arr. | Dep. |
|---|---|---|---|
| Jason Box | CU-Boulder | 3/23 | 6/23 |
| Nicolas Cullen | CU-Boulder | 3/23 | 6/23 |
| Konrad Steffen | CU-Boulder | 5/17 | 6/16 |
| Mike Jensen | CU-Boulder | 5/17 | 6/16 |
| Ben Balsley | CU-Boulder | 5/17 | 5/29 |
| Waleed Abdalati | NASA-GSFC | 5/17 | 5/29 |
| Jay Zwally | GSFC-NASA | 5/17 | 5/29 |

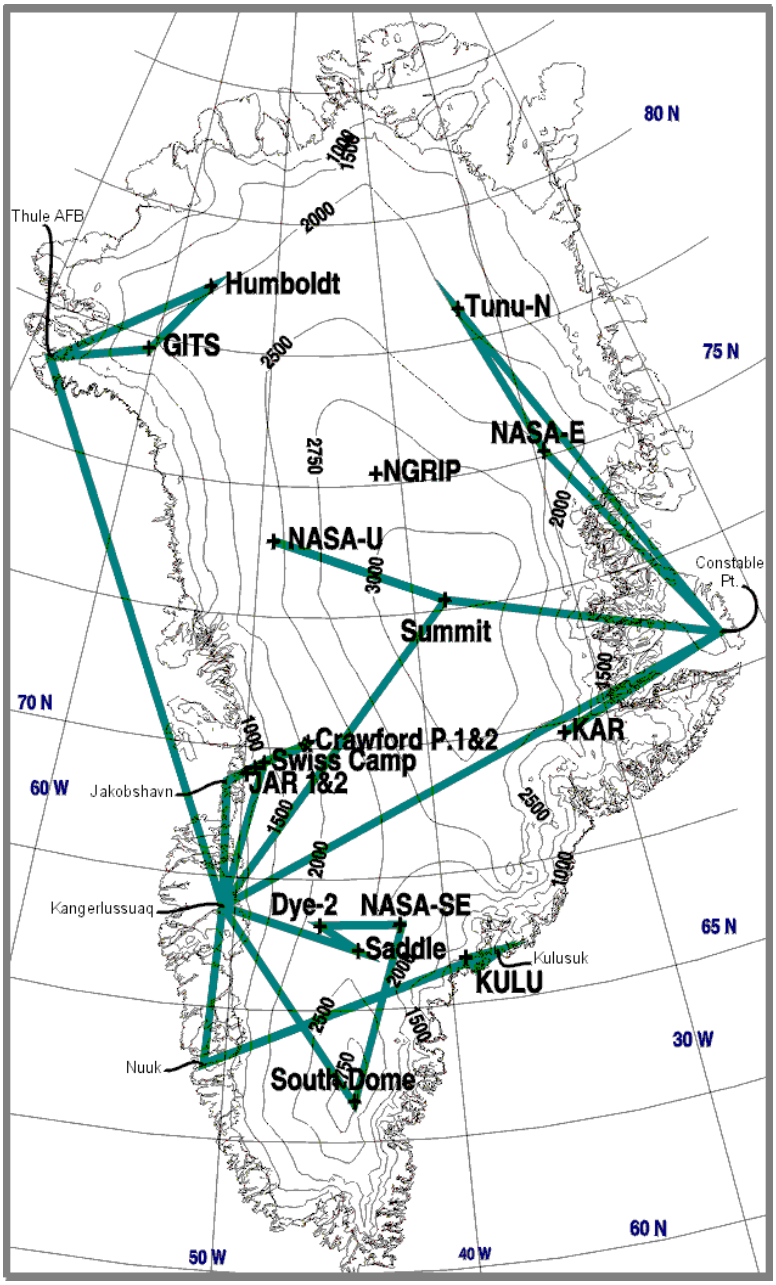


*Figure 1.1: Map showing the transit flights to the different AWS stations serviced in the '99 field season.*

# 2. GC-NET STATUS

## *2.1 Network Update*

During the 1999 field season, 17 of 18 AWS were visited for maintenance, installations, and calibration (Fig. 1.1). The AWS team was on the ice cap March 30th through June 23rd. AWS datasets collected in the field during the 1999 field season have replaced those transmitted datasets. The GC-Net archive has been brought up to date with a single common format for all station data. Compared with last year's 28 station years, there are now 50+ station years of GC-Net measurements processed and available for use (Fig. 2.1).

The ARGOS satellite data retrieval now updates automatically. Other steps in the data processing system have been refined and/or automated. The quality control procedures have been refined. More comprehensive documentation is available on station data sets. An HTML-based file server is in operational use internally.

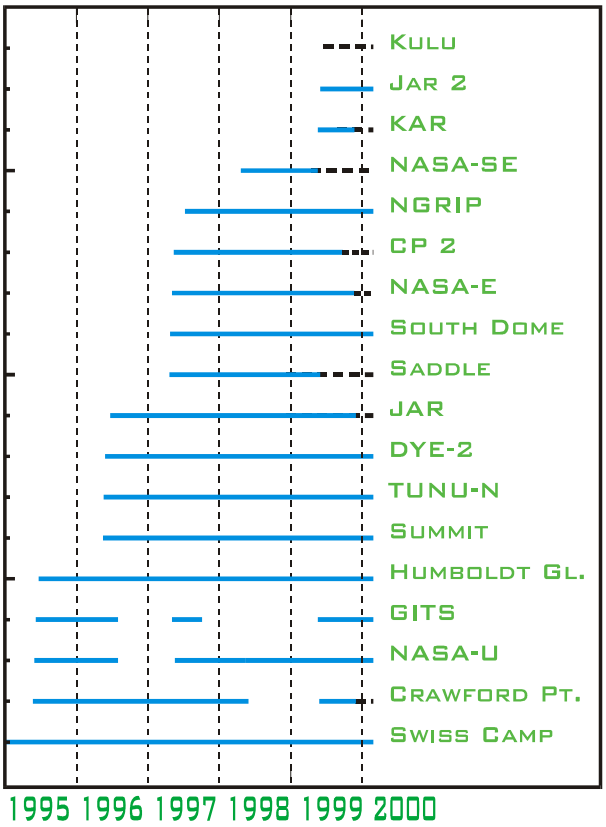


*Figure 2.1: GC-Net timeline. The dashed line indicates uncertain status due to no transmission.*

## *2.2 GC-Net Success Rate Statistics*

The statistics are based on 12 critical parameters such as: incoming shortwave radiation, reflected shortwave radiation, net radiation, temperature-humidity-wind profile at two levels, wind direction, pressure and surface height (Tab. 2.1). The possible data point count for all AWS and channels is $5.04574\ 10^6$, whereas $4.72291\ 10^6$ data were retrieved, resulting in an overall success rate of 93.6%.

*Table 2.1: GC-Net success rate statistics*

| **Year** | **1995** | **1996** | **1997** | **1998** | **1999** |
|---|---|---|---|---|---|
| Swiss Camp | 60.23 | 76.39 | 99.88 | 94.27 | 92.27 |
| Crawford Pt. | 98.50 | 90.58 | 77.26 | 55.17 | 40.56 |
| NASA-U | 98.93 | 56.38 | 61.87 | 99.94 | 92.54 |
| GITS | 98.99 | 98.50 | 56.36 | 0.00 | 55.19 |
| Humboldt Gl. | 99.80 | 97.01 | 99.06 | 99.47 | 96.52 |
| Summit | | 96.47 | 89.38 | 86.97 | 88.62 |
| TUNU-N | | 99.91 | 92.48 | 93.36 | 91.09 |
| DYE-2 | | 99.88 | 99.89 | 99.86 | 98.20 |
| JAR | | 99.97 | 99.87 | 99.97 | 97.94 |
| Saddle | | | 90.46 | 96.20 | 99.39 |
| South Dome | | | 83.29 | 87.33 | 86.03 |
| NASA-E | | | 99.29 | 90.61 | 90.39 |
| CP2 | | | 99.56 | 99.55 | 91.55 |
| NGRIP | | | 99.20 | 96.97 | 94.37 |
| NASA-SE | | | | 99.25 | 99.98 |
| KAR | | | | | 91.58 |
| JAR2 | | | | | 95.33 |
| **Annual** | **87.26** | **91.93** | **93.12** | **94.02** | **93.60** |

## *2.3 Quality Control*

Quality control procedures have been revised and applied to GC-Net archived data and transmissions through the end of 1999. Recent quality control improvements include a new quality identifier to represent questionable wind profile data resulting from contamination by the AWS mast. Another data quality improvement is a temperature instrument correction for cases when solar overheating occurs (Fig. 2.2).

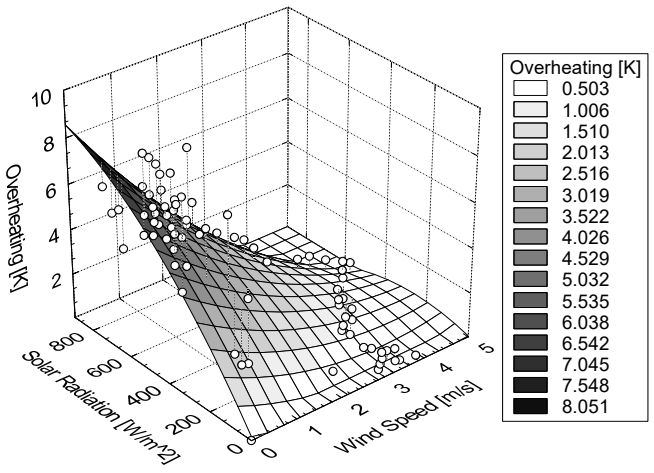


*Figure 2.2: Temperature instrument correction as a function of solar radiation and wind speed derived from the observed difference between ventilated and non-ventilated temperature sensors.*

Data for Figure 2.2 were obtained from field experiments in Greenland in 1999.

$$Correction = 0.201-0.813*W+0.014*S+0.165* W^2 -0.002* W *S-4.742e-6*S^2$$

where $W$ is wind speed in m $s^{-1}$and $S$ is the solar radiation in W $m^{-2}$. This correction is applicable to the Young UT-12P radiation shield with Vaisala-CS-500 temperature-humidity instruments.

## *2.4 Humidity Data Correction*

The probe used by the GC-Net measures relative humidity (RH) scaled with respect to liquid water. However, for meaningful humidity measurements at temperatures below 0 °C, the raw data must be rescaled to reflect saturation with respect to ice. The theory and methods to rescale RH values for saturation with respect to ice are reviewed by Anderson (1994). The conversion is made in two steps. The first step is to multiply each RH reading by the ratio of saturation vapor pressure with respect to water over that with respect to ice at that air temperature. The humidity readings were also rescaled with reference to the maximum output of the sensor for a given 1 K bin in temperature. The 96$^{th}$ percentile of each sorted bin is taken as the maximum output of the sensor since occasional (spuriously) high readings can occur in the course of 1-year hourly measurements. Makkonen (1996) has pointed out that this correction neglects the potential for supersaturation with respect to ice. Anderson (1996) showed that supersaturation cases occurred a few percent of the time.

## *2.5 New AWS Stations*

Three new sites were added to the GC-Net: (1) an eastern Greenland accumulation zone site on the northern rim of the Kanderlussuaq glacier basin (KAR), (2) A western Greenland ablation region of the Jakobshaven Glacier at 600 m elevation (JAR2), and (3) near Kulusuk at 800 m elevation on the northern rim of a surging glacial basin (KULU). The location of the new station are given in Figure 1.1.

## *2.6 AWS GPS*

As part of 1999 field work, GC-Net stations were equipped with GPS circuitry. GPS are used for daily clock synchronization to eliminate AWS clock drift and subsequent loss of satellite data link. We will begin to log the AWS position as part of the regular measurement routine in effort to measure ice motion and the ever-changing AWS horizontal position and elevation.

## *2.7 Automated WWW Plots*

Recent 6 days of hourly surface meteorological ASCII data and plots are updated hourly on the WWW at: http://cires.colorado.edu/steffen/aws/current_GC-Net_plots.html (Fig. 2.3). The GC-Net sites that are using GOES and ARGOS satellite data links are operationally updating automatically as of September 16 1999.

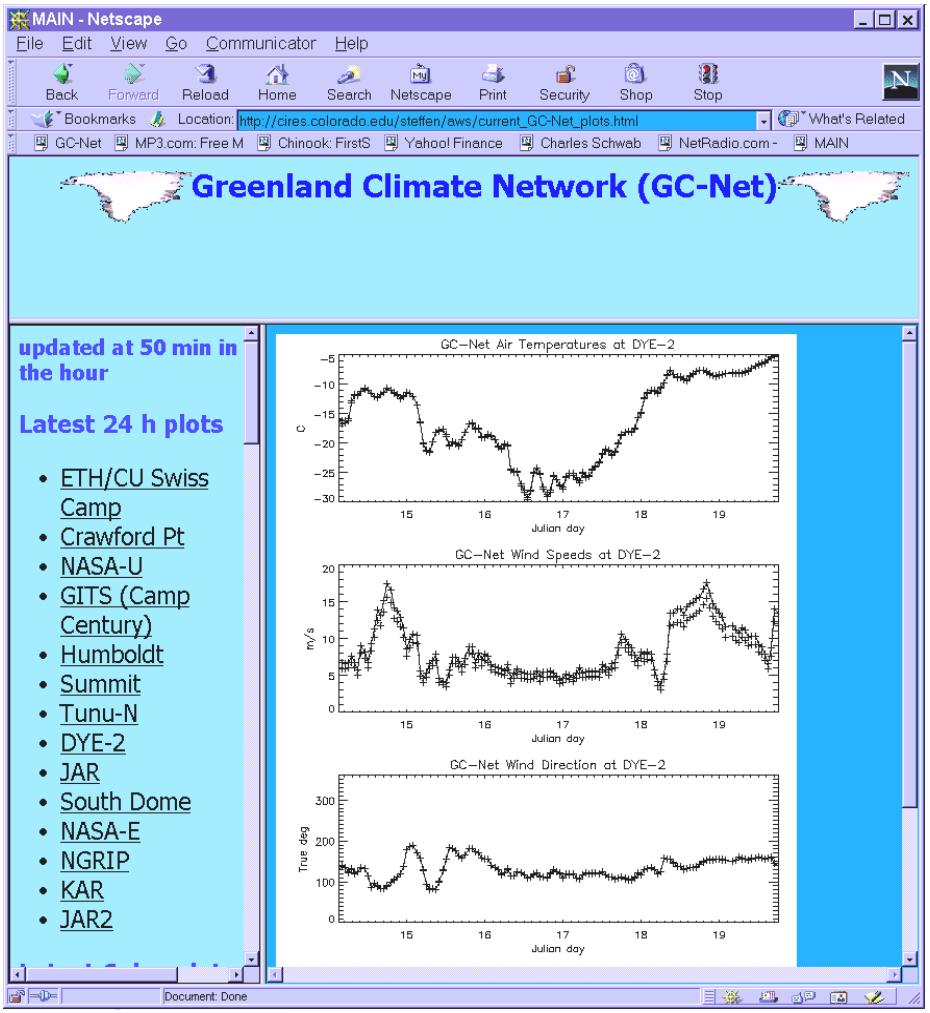


*Figure 2.3: Sample plot of the GC-Net data web site with near-real time data for a six-day period.*

# 3. RESULTS

## *3.1 Sublimation*

### *3.1.1 Calculation*

The mass balance of the Greenland ice sheet affects both global sea level and ocean circulation. Yet, the magnitude of the moisture flux to and from the ice sheet surface via sublimation is a relatively poorly known component of the mass balance. Variations in sublimation caused by climate changes will affect accumulation rates. Sublimation estimates are used to gauge the sensitivity of the surface mass balance to climate fluctuations such as temperature and specific humidity. Water vapor fluxes are determined using aerodynamic profile methods corrected for atmospheric stability variations.

Sublimation is directly related to the vertical specific humidity gradient (dq/dz) (Fig. 3.1). The vertical humidity gradient shows that sublimation losses are greatest in summer months, while small amounts of deposition occur in winter at some sites.

### *3.1.2 Method*

Five methods to calculate the sublimation moisture flux are being evaluated (Tab. 3.1). These rely on the direct relationship between the latent heat flux and sublimation. The evaporative mass transfer *(dM)* is the latent heat flux *($Q_{LH}$)* multiplied by the time change *(dt)* and divided by the latent heat of sublimation *($L_s$)*.

$$dM = \frac{Q_{LH}\,dt}{L_s}$$

For temperatures greater than or equal to 0° C, the latent heat of fusion is used.

*Table 3.1: Profile-based Sublimation Methods*

| Method | Equation | Source |
|---|---|---|
| Saturation Method 1 (s1) | $Q_{LH} = -\rho u_*^{\,2}\left[q_z - q_0\right]u_z^{\,-1}\Phi_M$ | (Lettau, 1979) |
| Saturation Method 2 (S2) | $Q_{LH} = -LD\rho\dfrac{0.622\left(e_z - e_0\right)\Phi_M}{p}$ | (Deardorff, 1968), D is an exchange coef. given by $D_0 = \dfrac{k^2 u_z}{\left(\ln z - \ln z_0\right)}$ |
| Aerodynamic Profile Method (AM) | $Q_{LH} = -\rho_{air} L k^2 \Delta\overline{q}\Delta\overline{u}\left(\left(\ln z_2/z_1\right)^{-2}\Phi_M^{\,-2}\right)$ | (Oke, 1987) |
| K-Theory (KT) | $Q_{LH} = -KL\rho\dfrac{\overline{q_2} - \overline{q_1}}{z_2 - z_1}\Phi_M$ | (Dyer 1974), K is an exchange coefficient taken as a constant. |
| Drag Method (D) | $Q_{LH} = -C_e\rho\overline{u_z}\left(\overline{q_z} - \overline{q_0}\right)c\Phi_M$ | (Brutsaert, 1982), c is the conversion factor from evaporation rate to latent heat flux. $C_e$ is the drag coefficient, taken as a constant. |

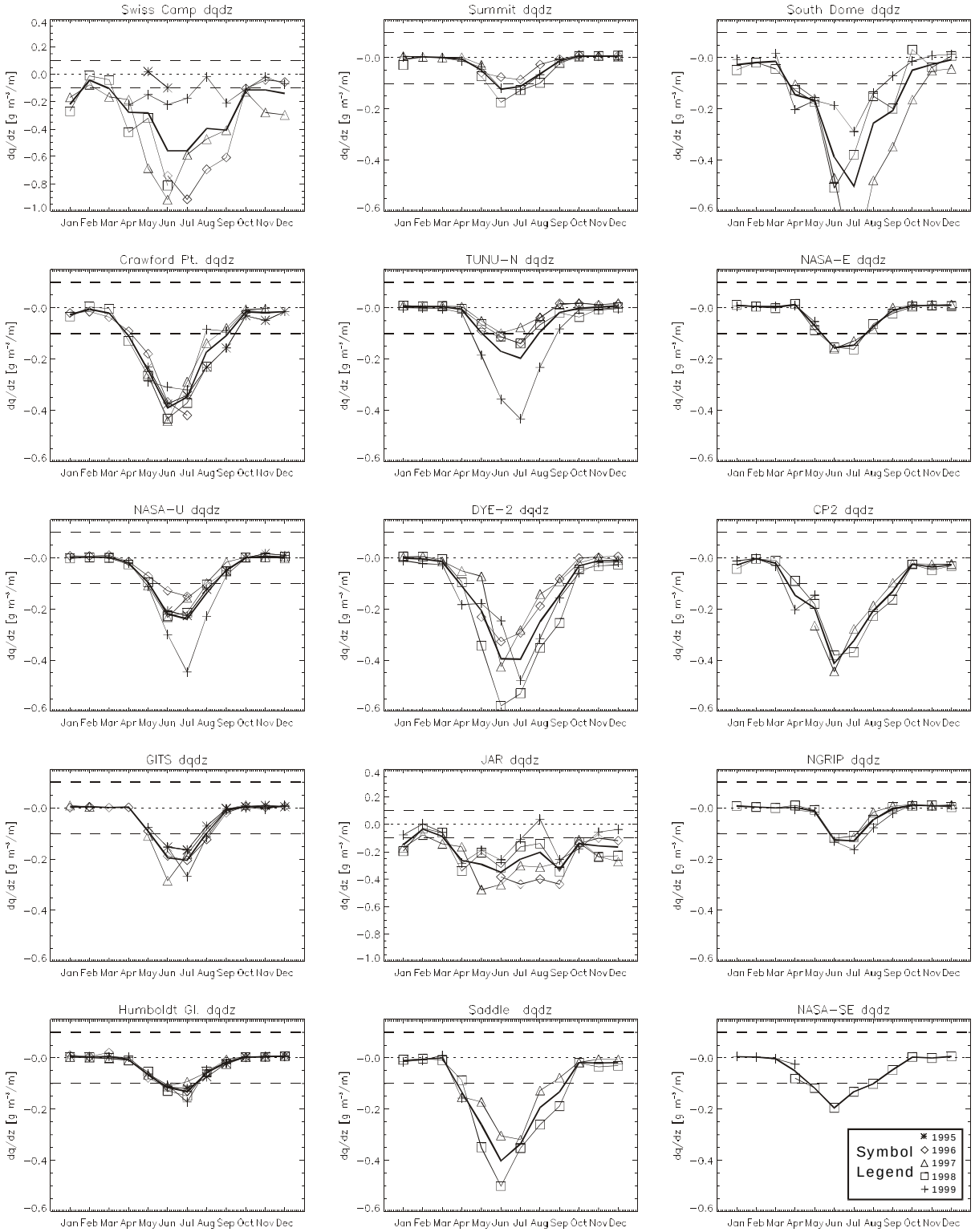


*Figure 3.1: Seasonal cycles of vertical humidity gradient over the Greenland ice sheet surface based on GC-Net measurements. Dashed lines indicate the relative accuracy of the humidity measurements ($\pm 0.1$ g m$^{-3}$). Thick solid lines indicate the average of available monthly means.*

The various methods have in common the vertical specific humidity gradient $\left(\overline{q_z} - \overline{q_0}\right)$ or the vertical water vapor pressure gradient $\left(e_z - e_0\right)$. Other micrometeorological parameters include the wind speed ($u$), sensor height ($z$), the friction velocity ($u_*$), air density ($\rho$), and roughness length ($z_0$). $\Phi_M$ is a stability function that scales the neutral-stability turbulent heat fluxes in terms of atmospheric stability variations. $\Phi_M$ is not well defined for ice sheet atmospheres which tend to be very stable throughout the year. Using $\Phi_M$ that has been developed for land surfaces have been found to introduce uncertainty and in some cases definite error. Hence, $\Phi_M$ will be examined in future field experiments.

### *3.1.3 GISS-99 Modeled Evaporation Rates*

A 50-year time series of evaporation rates on a 4x5 degree grid from the Greenland region were extracted from the NASA GISS SI99 B384 global climate model (Hansen et al., 1997) http://www.giss.nasa.gov/data/si99/results/ (James Hansen, jhansen@giss.nasa.gov). The GISS model has 12 atmospheric layers and includes well-mixed greenhouse gases, tropospheric aerosols, stratospheric aerosols, and ozone changes. Fifteen grid cells are located within the Greenland region (Fig. 3.2). Of the 15 cells, 3 have a small amount of land in them corresponding to the South Dome, Kulu, and DYE-2 sites. Thirteen cells overlap with the GC-Net.

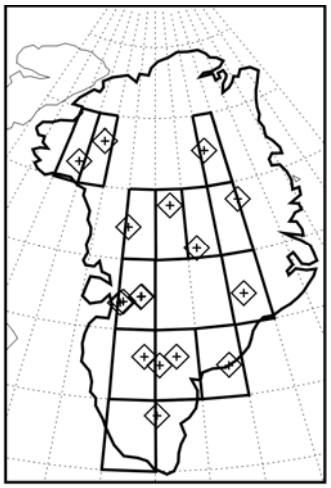

*Figure 3.2: GISS SI99 grid and GC-Net locations selected for comparison.*

The GISS model evaporation scheme (Deardorff, 1968) includes deposition. The same scheme has been run using GC-Net data. The results indicate that evaporation in the GISS model is smaller than that calculated from GC-Net data by 40%-100% (Fig. 3.3).

.

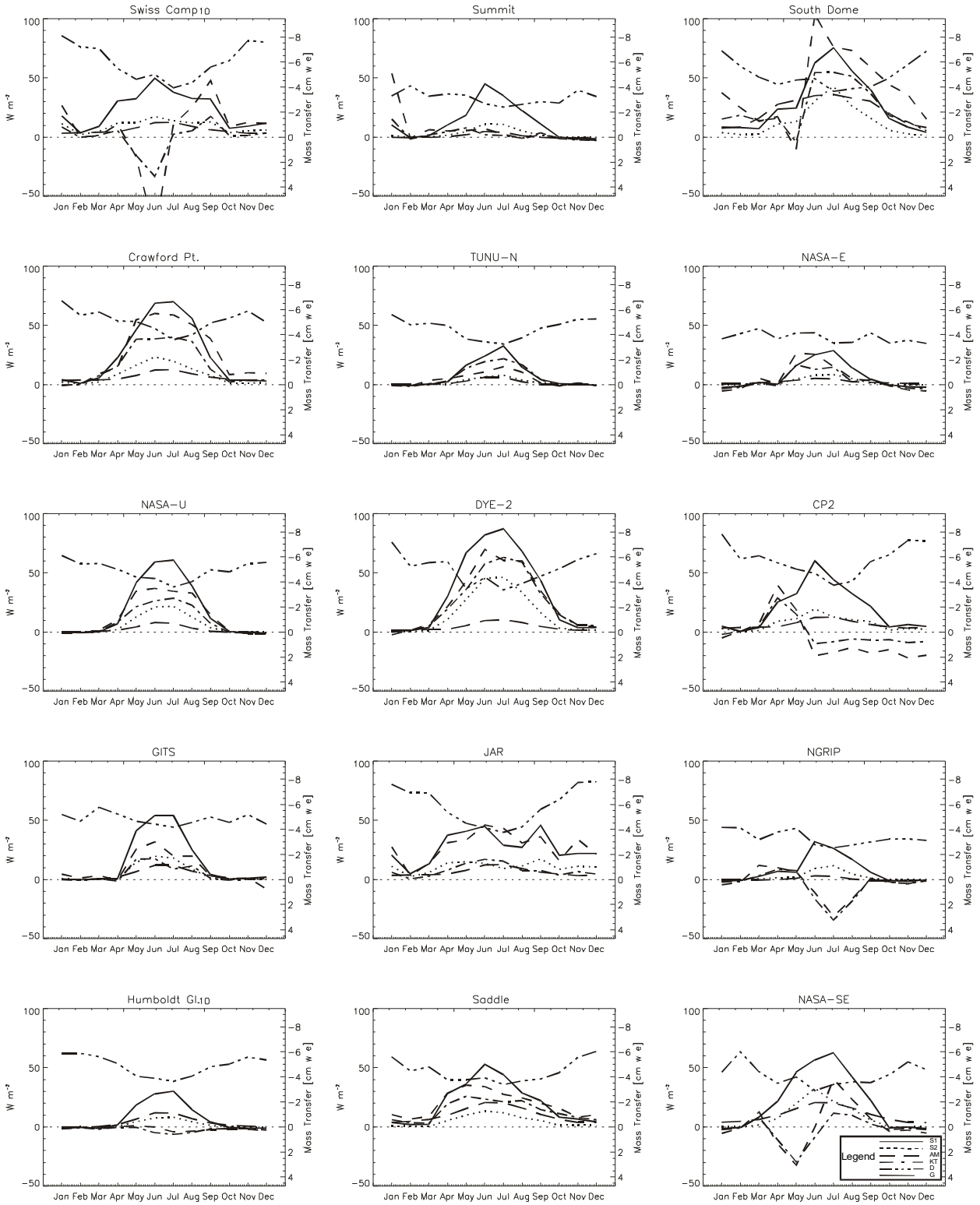


*Figure 3.3: Comparison of monthly mean sublimation rates derived from 5 methods using GC-Net observations.*

### *3.2 Snow Pits*

Density profiles from snow pits were measured at 11 AWS sites. With these, we will compare the accumulation history and water equivalence with sonic height records from GC-Net AWS. Samples were taken each 10 cm. If ice layers were present, representative samples were taken. Using the density profiles obtained from the 11 snow pits, depth-density relationships were derived (Fig. 3.4).

*Table 3.2: Snow density profiles collected at 11 AWS sites:*

| Site | Depth [m] | Date |
|---|---|---|
| Swiss Camp | 0.7 | Apr. 3 |
| NASA-SE | 1.7 | Apr. 21 |
| Saddle | 1.9 | Apr. 16 |
| South Dome | 1.6 | Apr. 22 |
| Crawford Pt. 1 | 1.2 | Apr. 26 |
| Summit | 1.8 | May 12 |
| Humboldt Gl. | 1.5 | Apr. 5 |
| GITS | 2.0 | Apr. 29 |
| DYE-2 | 0.9 | Apr. 18 |
| NASA-U | 2.0 | May 13 |
| CP-2 | 1.5 | May 28 |
| JAR | 1.2 | May 31 |

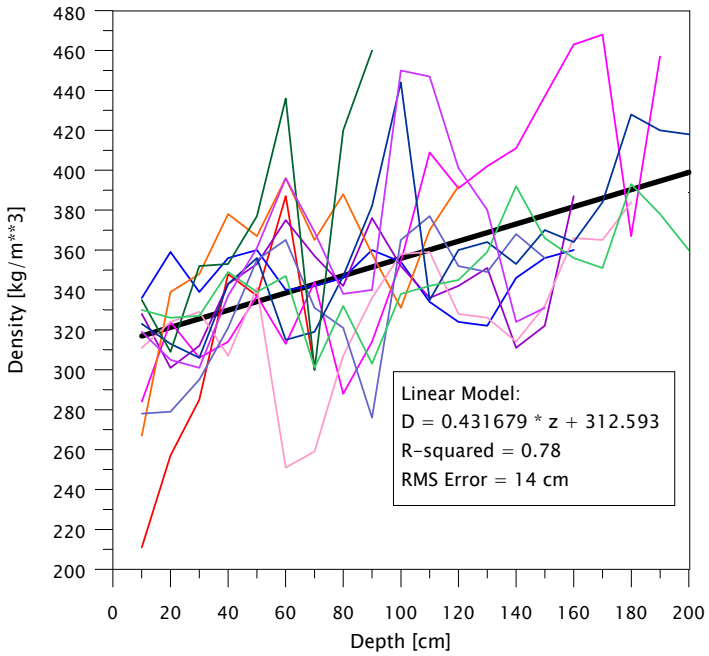


*Figure 3.4: Depth density relationship based on average snow pits density profile from 11 pits collected in 1999. D is the density and z is the depth coordinate.*

## *3.3 Comparison of the Bulk Aerodynamic and Eddy Correlation Methods*

Surface energy balance studies play a pivotal role in the understanding of surface processes linked with the Greenland ice sheet mass balance. The bulk aerodynamic method is the most practical micrometeorological technique to estimate turbulent heat fluxes over the Greenland ice sheet, as the only data requirements are temperature, humidity and wind speed in the surface layer. These meteorological parameters are now readily available over the ice sheet, being obtained from the automatic weather stations (AWS) deployed in association with the Greenland Climate Network (GC-Net). The eddy correlation technique was used to determine turbulent heat fluxes at the ice sheet mean equilibrium line altitude (Swiss Camp), about 89 km east of Jakobshavn at 69° 34' N, 49° 27' W. Comparison of the eddy correlation method to calculate sublimation and evaporation with two different bulk aerodynamic methods showed good agreement, with mean total errors less than 8% for both methods. The sensitivity of the two bulk aerodynamic methods to measurement error is described to account for the differences in calculated water equivalent loss. The better estimates of sublimation and evaporation using temperature, humidity and wind speed measurements at two heights in the atmosphere supports the decision to maintain a two level profile on the network of AWS over the Greenland ice sheet.

### *3.3.1 Methodology*

This present work examines some of the problems involved in deriving estimates of the surface energy exchanges at the ice sheet mean equilibrium line altitude by comparing the eddy correlation and bulk aerodynamic techniques during stable atmospheric conditions. The approach taken is to compare a number of different methods to permit an evaluation of the most appropriate method to improve estimates of evaporation and sublimation over the Greenland ice sheet.

Experiments were designed to enable the comparison between turbulent heat fluxes obtained from the eddy correlation and bulk aerodynamic techniques. The eddy correlation system was in operation between 25 May and 10 June, 1999, while energy budget measurements used for this comparison were made during the period 30 May to 2 June, 1999.

*The eddy correlation method (EM)*

The eddy correlation method (EM) measures turbulent fluctuations in vertical wind speed (w), air temperature (T), and humidity ($\rho_v$) from which the turbulent sensible heat ($Q_H$) and latent heat ($Q_E$) fluxes are determined:

$$Q_H = \rho_a \, c_a \, \overline{w'T'} \tag{1}$$

$$Q_E = L_V \, \overline{w' p'_v} \tag{2}$$

where primes denote instantaneous departures from mean quantities, overbars denote covariances, $p_a$ is the density of air (kg $m^{-3}$), $c_a$ the specific heat of air at constant pressure (J $kg^{-1}$ $K^{-1}$), and $L_v$ the latent heat of vaporization (J $kg^{-1}$). The sign convention employed is that the non-radiative fluxes directed away from a surface are positive.

*The bulk aerodynamic profile method (BPM)*

The technique to derive the turbulent heat transfers of $Q_H$ and $Q_E$ using measurements of temperature, humidity and wind speed at two heights in the atmosphere is an approach used by Steffen (1995), and described by Oke (1987):

$$Q_H = - c_a k^2 z^2 \left(\frac{\Delta \bar{u}}{\Delta z} . \frac{\Delta \bar{\theta}}{\Delta z}\right) (\phi_M \, \phi_H)^{-1} \tag{3}$$

$$Q_E = -L_v\, k^2 z^2 \left(\frac{\Delta \bar{u}}{\Delta z} \cdot \frac{\Delta \overline{p_v}}{\Delta z}\right)(\phi_M\ \phi_V)^{-1} \quad (4)$$

where Δ denotes the difference or net change in a quantity at the two profile heights, the overbar denotes the mean value of an entity, k the von Karman's constant (0.4 m), z the profile height height (m), *u* the horizontal wind speed (m $s^{-1}$), θ the potential temperature (K), $p_v$ the density of water vapor (kg $m^{-3}$) and $\phi_M = \phi_H = \phi_V$ are the dimensionless stability functions to account for the curvature of the logarithmic wind profile due to bouyancy effects. Empirical evidence leads to the following description of the stability function used in equations (3) and (4) (Steffen, 1995):

$$(\phi_M\ \phi_X)^{-1} = (1 - 5.2\, Ri)^{-1} \quad 0 < Ri < 0.19 \quad (5)$$

where $\phi_X$ is either the stability function for heat ($\phi_H$) or water vapor ($\phi_V$) and Ri the Richardson Number defined by:

$$Ri = \frac{g}{\bar{\theta}} \cdot \frac{(\Delta \bar{\theta} / \Delta z)}{(\Delta \bar{u} / \Delta z)^2} \quad (6)$$

where the overbar denotes the mean value of an entity, g is the acceleration of gravity (m $s^{-2}$).

*The simple bulk transfer method (STM)*

The second approach to calculate the heat transfers of $Q_H$ and $Q_E$ used bulk aerodynamic formulae, which were derived by combining flux-gradient formulae with empirical log-linear profile forms (Deardorff, 1968). These formulae have been applied over snow and ice by a number of authors, including Price and Dunne (1976), Moore and Owens (1984), Hay and Fitzharris (1988), and Ishikawa *et al.* (1992). The formulae used are:

$$Q_H = \rho_a\, c_a\, D_H\, (\theta_z - \theta_o) \quad (7)$$

$$Q_E = \rho_a\, L_v\, D_E\, (0.622 / P_a)(e_z - e_o) \quad (8)$$

where $\theta_z$ is the potential temperature (K) at height z (1.35 m), $\theta_o$ the surface potential temperature (K), $P_a$ the atmospheric pressure (hPa), $e_z$ the vapor pressure at height z (hPa), $e_o$ the vapor pressure at the surface (hPa), and $D_H$ and $D_E$ the bulk exchange coefficients for heat and water vapor, respectively (m $s^{-1}$). The values of potential temperature at the surface were determined from the natural logarithm (a least squares regression fit) of potential temperature at the two profile heights, and the surface potential temperature was used to derive the vapor pressure of the snow and ice surface (Stearns and Weidner, 1993). Under neutral conditions $D_H$ and $D_E$ are assumed from similarity arguments to equal $D_O$ (Stull, 1988), the momentum exchange coefficient, which is given by:

$$D_O = \frac{k^2\, u_z}{(\ln(z / z_o))^2} \quad (9)$$

where $u_z$ is the wind speed at height z (m $s^{-1}$), z the measurement height (1.35 m), and $Z_O$ the roughness length (m). The exchange coefficients were corrected for non-neutral atmospheric conditions using the stability function equation (5), where the Richardson Number is defined by equation (6). The roughness height was obtained from wind speeds ($u_{1,2}$) at two heights ($z_{1,2}$) for each period under neutral conditions (| Ri |) < 0.01) using the equation:

$$Z_O = \exp\left(\frac{(u_2 \ln z_1 - u_1 \ln z_2)}{(u_2 - u_1)}\right) \quad (10)$$

The value of $Z_O$ calculated from equation (10) is very sensitive to errors in the wind speeds. Regression analysis and visual examination of the time series of $Z_O$ and ln$Z_O$ showed no simple trends with time. Because of these factors, the median value of $Z_O$ was considered representative of the entire period ($1.01 \times 10^{-3}$ m), which is comparable to other $Z_O$ values proposed over snow and ice.

### *3.3.2 Instrumentation*

The primary flux measurement system at the ice sheet equilibrium line altitude site was a Campbell Scientific Inc. (CSI) eddy covariance (EC) system. A three dimensional sonic anemometer (CSAT3, CSI) with a fine wire thermocouple (FW05, CSI) and an ultraviolet hygrometer (KH20, CSI) were mounted on a cross arm at 1.5 m height on a permanent mast 20 m from the automatic weather station (AWS). Supporting measurements for EC were relative humidity and air temperature, also measured at 1.5 m (HMP35C, Vaisala, Finland) and atmospheric pressure (SBP 270, Setra). The EC measurements had a 0.1 second execution interval (10 Hz), with ten minute averages logged by a CR21X datalogger (CSI), and averaged to sixty minute means to coincide with the AWS fluxes. The measured latent heat flux was corrected for the effects of a non-zero mean vertical wind speed due to air density fluctuations caused by the convective fluxes (Webb *et al*., 1980) and for oxygen absorption effects following Tanner and Greene (1989) and Kelliher *et al*., (1997). These corrections typically increased the latent heat flux by 4-8% over the measurement period.

Measurements for the two aerodynamic methods were obtained from a permanent automatic weather station (AWS) installed in conjunction with the Greenland Climate Network (GC-Net). Temperature, humidity (CS500, CSI) and wind speed (05103, R.M. Young Wind Monitor) were measured at mean heights of 1.35 and 2.55 m, respectively. Changes to the measurement heights were corrected using a sonic ranging sensor (SR50, CSI). Relative calibration of the profile instruments was conducted before the measurement period. Supporting measurements for the analysis were net all-wave radiation (Q*7.1, REBS) and pressure (CS105, CSI). The effects of wind on the REBS (Q*7.1) net pyradiometer were corrected for both positive and negative net flux conditions. The measurements of temperature and humidity had 60 second execution intervals, net all-wave radiation and wind speed 15 second execution intervals, while pressure was sampled on the hour with the sixty minute averages logged for all instruments by a CR10X datalogger (CSI).

### *3.3.3 Results*

Figure 3.5 shows that the major meteorological parameters at the study site had a distinctive diurnal pattern during the measurement period. The net all-wave radiation was primarily negative (mean value of –24.5 W $m^{-2}$), with small positive values between approximately 1000–1800 GMT (Fig. 3.5a). The mean wind speed was 7.7 m $s^{-1}$, with the highest values at the beginning of the measurement period. During conditions when wind speeds were greater than 10 $ms^{-1}$ considerable transport of snow over the ice sheet surface was observed. Temperature and vapor pressure were typically highest between approximately 1400-2000 (Fig. 3.5c, d), with mean values over the entire period –4.1 °C and 3.8 hPa, respectively. Figure 3.6 shows that the structure of the surface boundary layer, as a function of the Richardson number, was stably stratified during the measurement period. The moderate to strong winds associated with the katabatic flow created a wind shear large enough to maintain a continuously turbulent state.

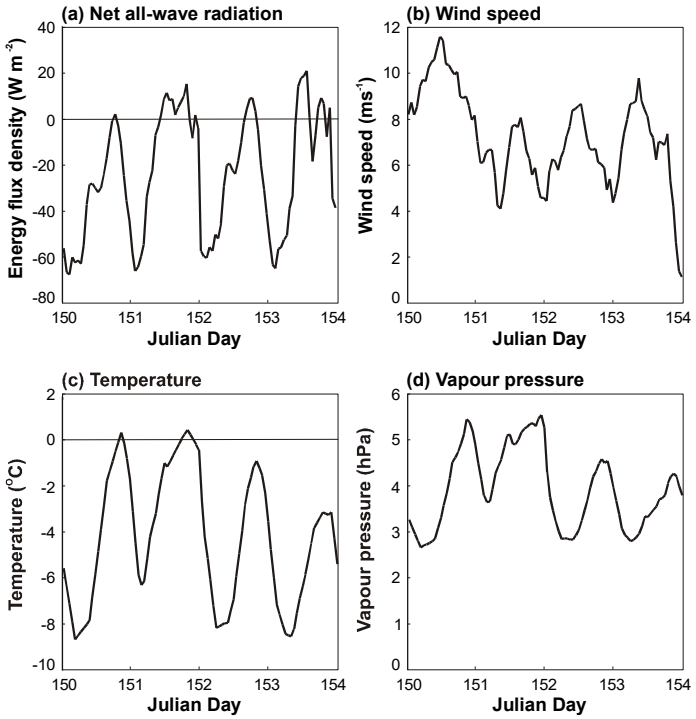


*Figure 3.5: Time series of the major meteorological parameters during the measurement period (30 May – 2 June). Measurements of wind speed, temperature and vapor pressure are taken from the lower profile height (1.35 m above ground surface).*

Figure 3.7 shows the time series of the sensible and latent heat fluxes, where EM is the eddy correlation method; BPM the bulk aerodynamic profile method and STM the simple bulk transfer method. The EM sensible heat flux was strongly negative at the beginning of the measurement period (Fig. 3.7a), which provided energy to the surface for sublimation. The EM sensible heat flux gradient remained towards the surface throughout the period except for a short time between 1200-1400 on Julian Day 153. The BPM sensible heat flux showed a similar trend to the EM sensible heat flux but tended to be greater in strength over the period, with the mean BPM value 22% greater than EM (Tab. 3.3). The BPM value became positive for a short period on Julian Day 151 and remained positive after 1200 GMT on Julian Day 153, with a maximum of 18.3 W $m^{-2}$. In contrast, the calculated STM sensible heat flux was of much smaller magnitude, with a mean value of –3.8 W $m^{-2}$. Even though the magnitude of the STM sensible heat flux was significantly lower it remained in phase with the EM sensible heat flux. Figure 3.7b shows that the EM latent heat flux was greatest at the beginning of the measurement period, with a maximum value of 93.4 W $m^{-2}$, and became negative (a gradient towards the surface) typically between 0-600 on Julian Days 151-153. The BPM and STM latent heat fluxes were in the same phase as the EM latent heat flux during the measurement period but typically had more moderate values, with their respective ranges 68.1 and 73.7 W $m^{-2}$, respectively, approximately 25% less than the EM range (Tab. 3.3). Unlike the EM latent heat fluxes the gradient of the BPM and STM latent heat fluxes remained away from the surface throughout the period (the BPM latent heat flux was briefly negative between 200-300 GMT on Julian Day 151).

The comparison of the EM sensible and latent heat fluxes with the BPM and STM methods is shown in Figure 3.8. The sensible heat fluxes derived from the BPM and STM methods both correlate well with the EM sensible heat flux values (Fig. 3.8a, b). Figure 3.8b shows that while the magnitude of the STM sensible heat fluxes are significantly smaller (concentrated around a mean value of –3.8 W $m^{-2}$) than the EM sensible heat fluxes the relationship between the two methods is nonetheless significant. The latent heat fluxes calculated using the BPM method shows a larger scatter against the EM latent heat fluxes than the STM method. While the magnitude of the calculated BPM and STM values are both smaller than the EM values, the cumulative sublimation and evaporation totals of the three methods over the measurement period are very similar (Fig. 3.9). Figure 3.9

shows that the water equivalent loss as calculated from the BPM and STM methods steadily increase, while the water equivalent loss from the EM method fluctuates in response to changes in gradient. The cumulative water equivalent loss totals as derived from the EM, BPM and STM methods over the measurement period are 3.45, 3.52 and 3.76 mm, respectively.

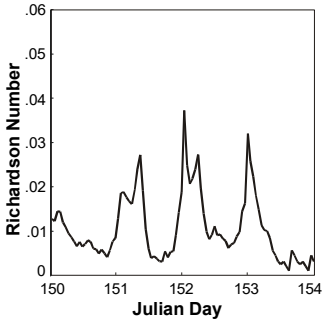


*Figure 3.6: The time series of stability (Ri) as determined from the profile measurements.*

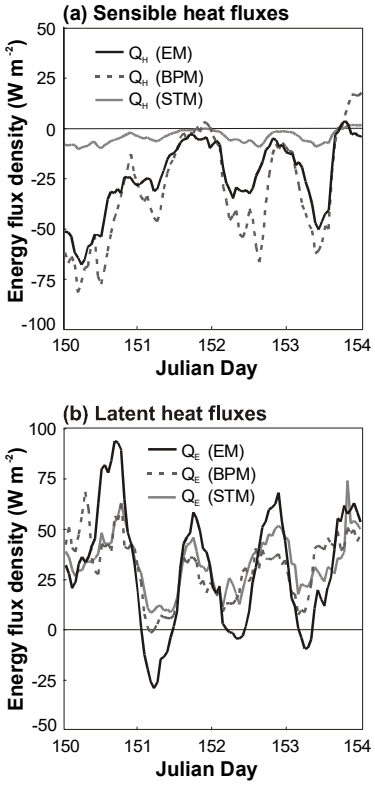


*Figure 3.7: The time series of the sensible and latent heat fluxes, where EM is the eddy correlation method, BPM the bulk aerodynamic profile method and STM the simple bulk transfer method.*

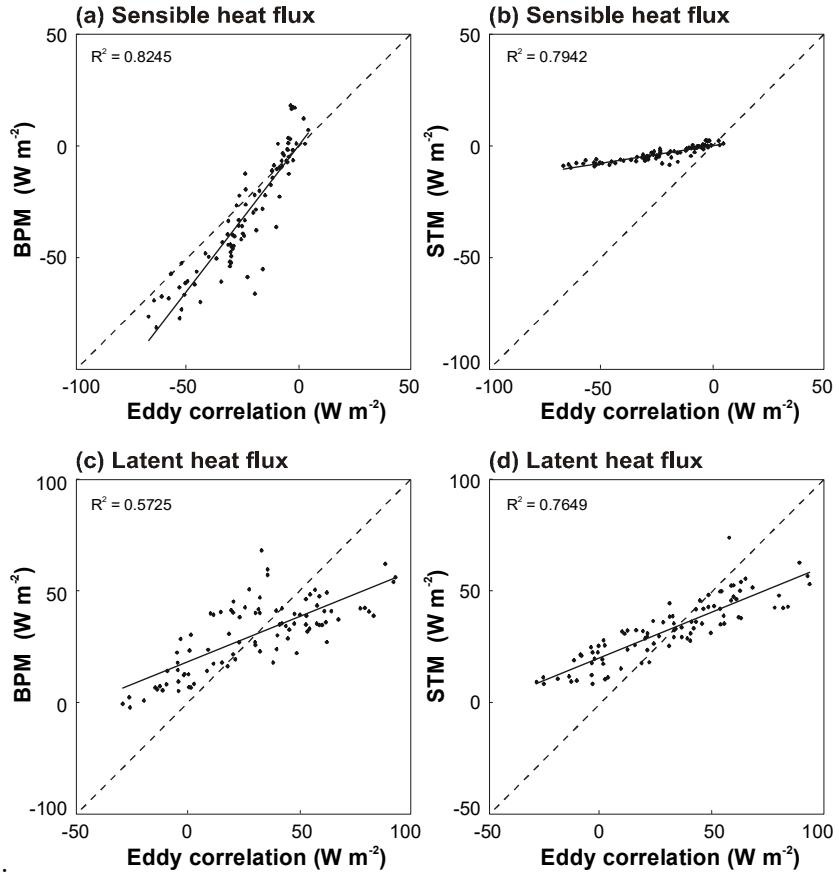


*Figure 3.8: Comparison of the eddy correlation (EM) sensible and latent heat fluxes with the bulk aerodynamic profile (BPM) and simple bulk transfer methods (STM). The dashed straight line plot shows the 1:1 relationship.*

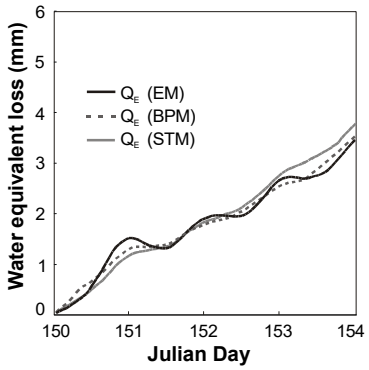


*Figure 3.9: The time series of cumulative water loss (mm) due to sublimation and evaporation during the measurement period.*

### *3.3.4 Discussion and conclusions*

Figure 3.7a shows that the calculated STM sensible heat flux is significantly underestimated using the STM approach but remains in phase with the other sensible heat fluxes. The calculation of the STM sensible heat flux is very sensitive to the difference in potential temperature as derived from equation (7). The primary control of the magnitude of the calculated STM sensible heat flux is the value of the momentum exchange coefficient, which is very sensitive to $Z_O$. If the value of $Z_O$ is increased by an order of magnitude the corresponding effect on the STM sensible heat flux is to double (about 53%) the value of $Q_H$. The STM sensible heat flux is very

similar to the EM and BPM sensible heat fluxes if $Z_O$ is increased by two orders of magnitude. The magnitude of $Z_O$ is very sensitive to wind speed and measurement height as derived from equation (10), which was also observed by Munro (1989) using comparable approaches to calculate $Z_O$.

The major difference between the EM latent heat flux and the BPM and STM latent heat fluxes was the tendency for the eddy correlation technique to show a moisture gradient towards the surface (negative EM values) typically between 0-600 GMT (Fig. 3.7b). In contrast, the humidity profiles from the AWS maintained a moisture gradient away from the surface for almost the entire measurement period, resulting in positive BPM and STM latent heat fluxes. Because the STM method is controlled by the assumption that the surface is saturated, the gradient away from the surface is maintained throughout the measurement period. However, the BPM method uses the measurements of humidity at two levels in the atmosphere and was briefly negative on Julian Day 151 (Fig. 3.7). The calculation of the BPM latent heat fluxes using equation (4) is very sensitive to changes in measurement height and gradients of water vapor density. For example, a change of $z_2$ by 0.05 m causes the BPM latent heat fluxes to decrease by approximately 15%. The more significant influence on the BPM latent heat fluxes is the sensitivity of the relative humidity measurements. An increase or decrease of relative humidity at either of the profile heights by an absolute value of 1% results in an error of ± 30%.

The BPM and STM methods to calculate water equivalent loss from the surface during stably stratified conditions compare favorably with the EM method (Fig. 3.8) despite sensitivity to the above measurement variables, with mean total errors of 2 and 8%, respectively. These results indicate that the calculation of water equivalent loss (or sublimation and evaporation) using the BPM and STM methods may be useful to derive longer term estimates of sublimation and evaporation. The advantage of utilizing the BPM method to estimate the turbulent fluxes is that knowledge of the surface characteristics (and calculation of the sensitive $Z_O$) is not required. The BPM method has the disadvantage that the values for temperature and moisture between two levels in the atmosphere can be difficult to resolve for small vertical gradients. The estimates of sublimation and evaporation using the BPM method supports the decision to maintain a two level profile on the network of AWS over the Greenland ice sheet deployed in association with the Greenland Climate Network (GC-Net).

*Table 3.3: General statistics for the time series of the sensible and latent heat fluxes using the eddy correlation (EM), bulk aerodynamic profile (BPM) and the simple bulk transfer (STM) methods (W $m^{-2}$).*

| ***Statistics*** | ***$Q_H$ (EM)*** | ***$Q_H$ (BPM)*** | ***$Q_H$ (STM)*** | ***$Q_E$ (EM)*** | ***$Q_E$ (BPM)*** | ***$Q_E$ (STM)*** |
|---|---|---|---|---|---|---|
| Number of obs. | 91 | 91 | 91 | 91 | 91 | 91 |
| Mean | -23.8 | -30.6 | -3.8 | 29.9 | 30.5 | 32.6 |
| Range | 71.7 | 99.5 | 12.2 | 122.6 | 70.0 | 65.4 |
| Minimum | -67.4 | -81.3 | -9.9 | -29.3 | -1.9 | 8.3 |
| Maximum | 4.3 | 18.3 | 2.3 | 93.4 | 68.1 | 73.7 |
| Standard deviation | 18.3 | 26.0 | 3.2 | 29.8 | 15.8 | 13.8 |

## *3.4 Tethered Parafoil Kites*

In May and June of 1999, Dr. Ben Balsley and one of his graduate students, Michael Jensen, joined members of Dr. Konrad Steffen's research group during a field campaign on the ice sheet of Greenland. Operations were conducted for roughly one month at the permanent meteorological station known as Swiss Camp. The goal of this field campaign was to test the feasibility of operating parafoil kite systems developed at the University of Colorado in the extreme environment of the arctic, under a variety of wind conditions. At the same time, an initial series of atmospheric data from the lowest few kilometers of the atmosphere was collected. This report summarizes the systems developed and used during the campaign, gives examples of the data collected, and takes a brief look at the potential of this technique for future research in the Arctic and Antarctic.

### *3.4.1 Development of a Tethered Parafoil System for Arctic Research*

Researchers at the Cooperative Institute for Research in Environmental Sciences (CIRES), at the University of Colorado in Boulder, have been heavily involved during the last decade in the design and use of parafoil kite and tethered balloon systems for making measurements in the lower atmosphere. Measurements of various atmospheric variables ranging from meteorological and microphysical to sampling of chemical species and even insect populations have been made at sites all over the world. Many of the research tools could be used in the Arctic with little or no modification, including the parafoil kites, Kevlar kite tether, and the atmospheric sensors and data telemetry systems. One major development required for the Greenland campaign was a new kite winching system.

Parafoil kites used were constructed of either ripstop nylon or polyester and contain no rigid structure to maintain their shape, only the pressure from the wind filling their open tubes. Parafoil kites are extremely efficient lifters, with the larger size ones (13 $m^2$) capable of producing a few hundred kilograms under strong winds of 15-20 m $s^{-1}$, while weighing less than 5 kg. A smaller size parafoil (Fig. 3.10), with an area of 7.3 $m^2$, was used during periods of higher winds. The parafoil kites proved to be very capable performers under the extremes of temperature and winds encountered during the experimental campaign.

*Figure 3.10: Preparation for launch a 7.3 $m^2$ parafoil kite.*

The kite tether used for the Greenland experiment was a braided Kevlar with a breaking strength in excess of 200 kg, a diameter under 2 mm, and a weight of 1.64 kg per km. This tether was chosen based on the capabilities of the 1-hp electric winch and a limited archive of historical upper air wind data for the experimental site.

The basic sensor pack consisted of a Vaisala RS-80 radiosonde with Tmax interface board, capable of providing real-time telemetered pressure, temperature, and relative humidity data and up to 6 additional channels of data at roughly 7.5-second intervals. During most flights, an Atmospheric Instrumentation Research (AIR) Humair probe was interfaced to the Tmax board to provide additional calibrated measurements of both air temperature and relative humidity. A second sensor pack for logging wind speed and direction, sensor pack pitch and roll angles,

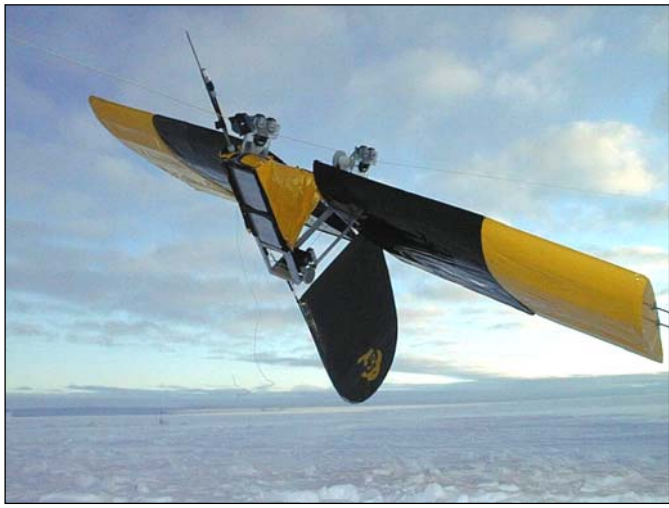

streamwise temperature and velocity fluctuations, and GPS position and speed was also test flown. Additionally, a single test flight of an off-the-shelf atmospheric aerosol sensor was also conducted.

A few flights of a prototype WindTRAM (Tether Rover for Atmospheric Measurements) were also made, providing relatively rapid profiles of basic meteorological variables. The WindTRAM (Fig. 3.11) travels along the kite tether using the power of the wind, by adjusting the angle of its wings under automatic control. A standard suite of sensors are built into the WindTRAM, include pressure, temperature, humidity, and wind speed, but the WindTRAM is also capable of carrying small (2-5kg, depending on the wind conditions), independent payloads suspended beneath it.

The workhorse of the CIRES kite system has been the truck/car winch, which uses a capstan attached to the raised drive wheel of a vehicle to control the kite tether and to let out and pull in the kite under high tensions. The inherent lack of vehicles on the ice sheet precluded using this system, and led to the development of an electric winch, which could be powered by a small gasoline generator. The winch used in Greenland (Fig. 3.12) was powered by a 1 hp, 3-phase electric motor, and included a failsafe brake, a 20:1 gearbox to reduce the motor speed and increase torque. This motor drove a 20 cm diameter capstan around which several wraps of the tether provided sufficient friction to power the kite tether in and out at tensions up to 180 kg and at speeds up to 1 m $s^{-1}$. An electromagnetic particle clutch was used to transfer a portion of the main drive motor's power to a small reel used to hold roughly 7 kilometers of Kevlar tether. A level-wind mechanism was used to insure that the tether was spooled cleanly on and off of the reel. The speed and direction of the winch was controlled using a hand-held control box.

*Figure 3.11: The WindTRAM*

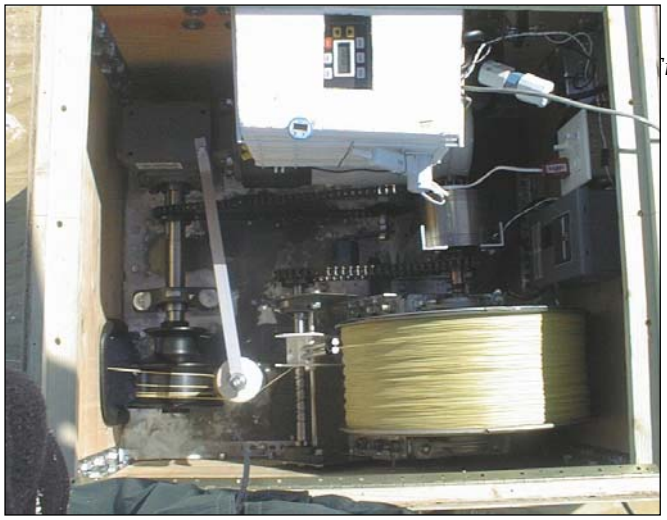

*Figure 3.12: The electric winch used during the Greenland campaign.*

### *3.4.2 Examples of Data Collected During the Campaign*

Over the course of the experiment, 15 individual flights were flown using the Vaisala radiosonde pack, with some flights carrying additional payloads, as well. Additionally, six WindTRAM flights were made, as well as five flights where high-frequency temperature and velocity fluctuations and/or GPS data were collected.

Two basic methods were used to collect data using the CIRES kite system. Most of the time the winch was fixed to the surface and the kites and instruments were flown using the prevailing wind. This method was effective for winds ranging from roughly 5 to 15 m $s^{-1}$, which were common during the experimental period. Alternatively, the winch and electric generator were fastened to a sledge and pulled behind a snowmobile. This technique generated a wind relative to the kite, allowing for easy launching and profiling. Lack of a dedicated sledge for this experiment and sufficient winds for surface-fixed launches most of the time, limited the use of this technique to a single day during the experimental period.

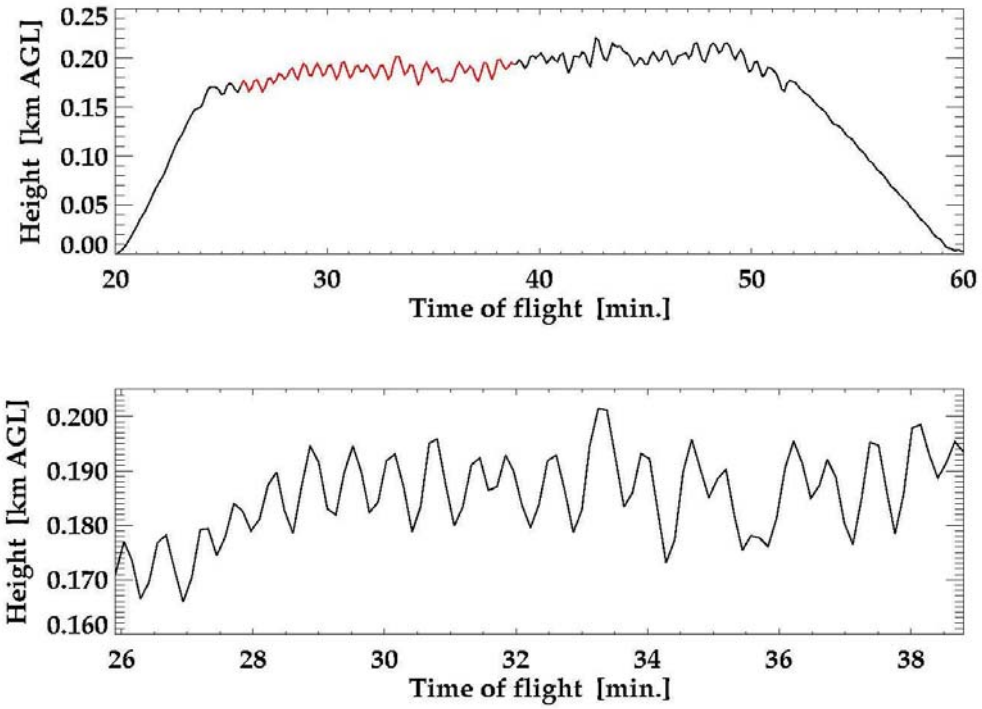


*Figure 3.13: Plots showing typical wave-like activity at the top of the katabatic flow. The top plot shows the full flight, and the bottom one shows the section highlighted in red from the first plot in greater detail.*

There were two primary meteorological conditions that dominated the fair weather periods during the time kite operations were conducted. The first condition was typified by a strong katabatic flow limited to the lowest few hundred meters above the surface. These flow conditions were characterized by a strong (typically, 10-20 m $s^{-1}$) jet in the first 200 to 300 meters and a rapid decrease in wind above that. This phenomenon created strong wave activity at the upper shear region of the jet, which is clearly identifiable in the altitude data, calculated using the pressure, temperature, and relative humidity data from the Vaisala radiosonde. Figure 3.13 shows a particularly clear example of this wave activity, during which flight of the kite was characterized by rapid ascents on the crests of the waves and then essential free-falls as the trough of the wave passed the kite and instruments. The regularity of these waves is made clear in Table 3.4, which shows the wave periods for a few of the Greenland flights.

The second flow regime extended to roughly 1.3 to 2 km and was encountered on 3 different occasions. During these episodes, measurements were made using the basic Vaisala pack, as well as a few rapid profiles using the WindTRAM. Figure 3.14 shows profiles of temperature and relative humidity obtained using the Vaisala radiosonde pack. The high vertical resolution is clearly evident from this plot.

During one of the few days when low winds and sledge availability allowed for testing of the towed system, a single profile to low altitude (~ 100 m) was made with the basic Vaisala and a separate datalogging system which recorded wind speed, direction and GPS position and velocity. The GPS sensor data is used to calculate the true wind speed and direction from the relative wind data collected from the moving instrument platform. In this case, the uncorrected GPS velocity data was used to gain an estimate of the wind profile (~±1 $ms^{-1}$), but a more accurate calculation could be made by differentially correcting the GPS measurements using data from a base station, such as the one continuously running at the Swiss Camp.

*Table 3.4: . Examples of observed wave activity*

| Flight | Date | Start time | Height | Wave period |
|---|---|---|---|---|
| SC106 | 01-Jun-99 | 17:55:11 | 0.20 km | 37 sec |
| SC113 | 09-Jun-99 | 3:46:10 | 0.15 km | 37 sec |
| SC114 | 09-Jun-99 | 5:37:02 | 0.18 km | 40 sec |
| SC115 | 09-Jun-99 | 16:15:48 | 0.04 km | 43 sec |

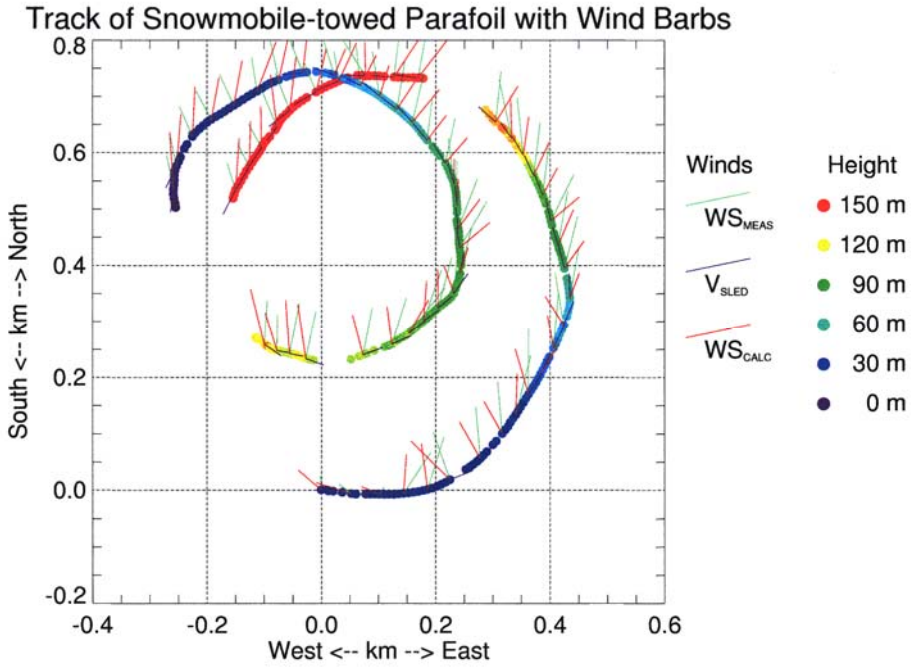


*Figure 3.14: Wind speed and direction measured from a kite launched from a snow mobile under calm wind conditions driving in a circle of 1 km around the Swiss Camp.*

### *3.4.3 Conclusions*

It is our feeling that the success of this initial attempt at extending the operating capabilities of the CIRES tethered parafoil systems into the Arctic has opened the door to a cost-effective, portable atmospheric profiling system that could greatly enhance airborne research at high latitudes. The CIRES group has conducted numerous experiments to measure chemical transport and emissions, meteorological variables, turbulent properties of the atmosphere, and other variables at sites all around the world. Using both the surface-fixed and towed parafoil systems, a variety of measurements could be made from essentially any snow or ice covered surface, under wind speeds ranging from 0 to 20 m $s^{-1}$. The altitude range of the measurements could extend from the surface to well into the free troposphere. We feel that the parafoil systems lend themselves to katabatic flow studies, aerosol and radiation measurements, as well as trace gas sampling and turbulence/flux measurements.

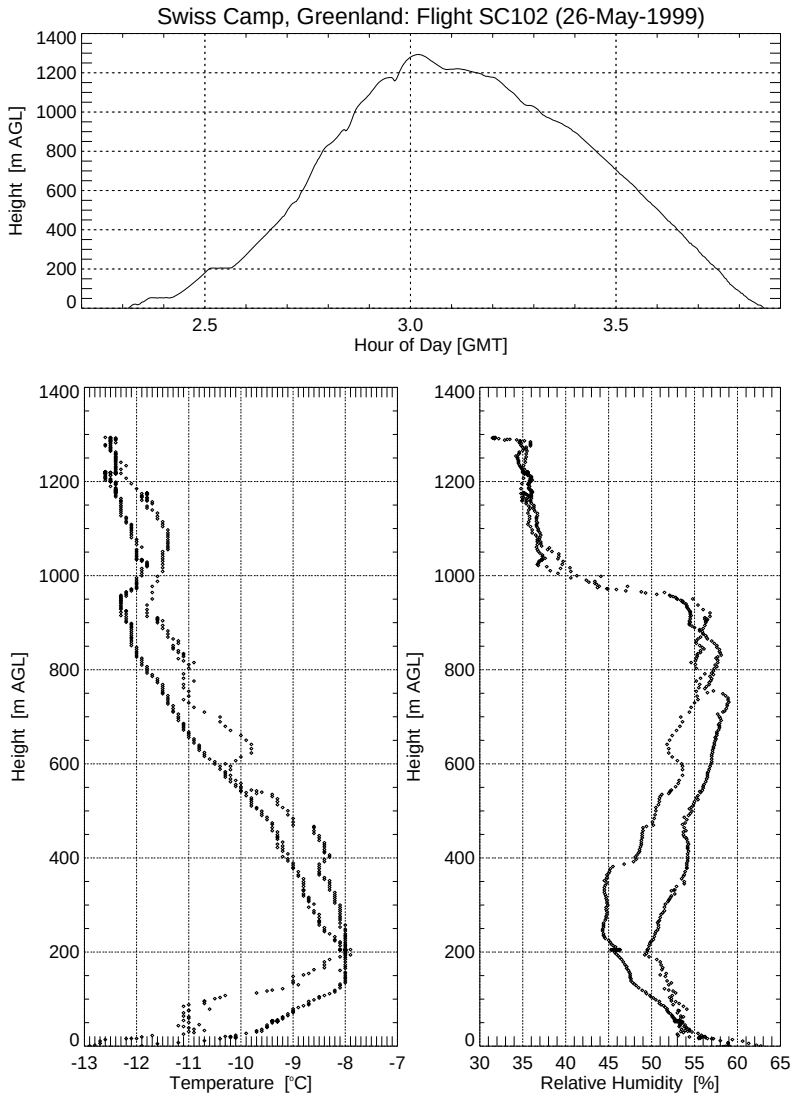


*Figure 3.15: Temperature and humidity profiles for the first 1.3 km above the Greenland ice sheet at the Swiss Camp based on an ascending and descending kite. The surface inversion near the ground was 5º C in the first 200 m.*

## *3.5 Terrestrial-Geodetic Investigations*

### 3.5.1 The geodetic program 1999

We performed geodetic measurements on the ground in order to determine height change, ice flow velocity and deformation (strain) in a test field around the ETH/CU-camp. This test field, consisting of a triangle with a central point, exists since 1991 and was re-measured in 1994, 1995, 1996 and 1999. Therefore, it is an excellent basis for determining mass balance parameters by terrestrial methods. A major point of interest is the reliability of GPS-measurements in Greenland. Four LEICA GPS-receivers from HfT Stuttgart were used, two of type System 200 and two of type System 300 (9500).

The geodetic program was performed in the period from July 21 to August 8, 1999. Due to significant of melt water, we had to fly daily by helicopter (Bell 206 Jetranger from Air Alpha) to the camp.

The measuring program included:

- Enlargement of the reference network in Ilulissat by 5 points, related to the old reference point EUREF 0112 near Hotel Arctic. The hotel is under construction, so the old fix-point might be destroyed soon. The network is used, too, for accuracy studies on short baselines.
- Static GPS baseline measurement Jakobshavn-Camp (JAV-Camp) at four days (27.7., 29.7., 31.7. and 3.8.99) over 6 hours each (10.00 a.m. – 16.00 p.m. local time), with a sampling rate of 15 seconds.
- Re-measurement of the actual positions of all the four points of the deformation network on the ice by GPS and tachometry. All old aluminum poles were found.
- Reconstruction and staking out of the old positions from 1991, 94, 95 and 96 by Real-Time-GPS. Re-measurement by GPS.
- Determination of the ice horizon by digging of snow pits.
- Topographical survey of the snow surface around the camp with gridding in distances of 100-200 m by GPS.
- Long-time GPS-measurements at the base station JAV-Youth Hostel in order to study ionospheric disturbances of GPS-signals.
- Testing a reflector less measuring electronic distance meter (ZEISS RecElta RL-S) when aiming on ice surfaces.

*Baseline Jakobshavn – Camp*

The accuracy of the baseline JAV-Camp is very important for comparisons of position and height on the ice. The baseline was measured at four days, for about 6 hours each. For calculation we used several software systems:

1. SKI 2.3, from LEICA,
2. Bernese Software 4.0, from University Bern (BGS 4.0),
3. GPSurvey 2.35, from TRIMBLE.

Even when using the same GPS-data, we got different results depending on the different software. We get the following discrepancies between the different software packets, using the Bernese software as a reference.

Especially in height we observed discrepancies of up to 2 decimeters. In spite of this, we used the SKI results (usually without ambiguity resolutions), because the studies from previous years were done with the SKI software. In general, the resulting surface height change is not subjective by the type of software.

Using the same software, the difference in heights for four days was small, with a standard deviation of ±0,025 m for the arithmetic mean, and we were able to resolve surface height changes between the different years.

*Table 3.5: Height discrepancies for the baseline Jakobshavn-Base Camp (Swiss Camp) using different sortware for data analysis.*

| JAV-Camp Campaign | BGS - SKI | | BGS - GPSurvey | |
|---|---|---|---|---|
| | Length (m) | Height (m) | Length (m) | Height (m) |
| 1995 | 0,00 | 0,24 | ---- | ---- |
| 1996 | 0,06 | -0.13 | ---- | ---- |
| 1999 | -0,02 | -0.11 | 0,02 | 0,03 |

The quality of GPS-data in Greenland is substantially worse than in Middle Europe. Firstly, the satellite orbits all have low inclination, in spite of numerous coverage. This constellation results in a poor height quality. Secondly, the satellite signal is disturbed by ionospheric scintillations, which cannot be modeled by 2-frequencies (L1, L2).

As an example Figure 3.16 depicts the ionospheric effects in Greenland. The upper part of the figure displays the total signal delay in the ionosphere, which ranges up to about 10 meters. But even more problematic are the short-termed random scintillations (middle part) ranging up to ±3 meters. The lowest part in Figure 3.16 shows the elevation angles of the satellites. The lower the elevation, the longer the path of the satellite signal is penetrating through the ionosphere, and the greater will be the disturbances. In contrast, we see much smaller and calmer effects in central Europe (e.g., Stuttgart) (Fig.3.17).

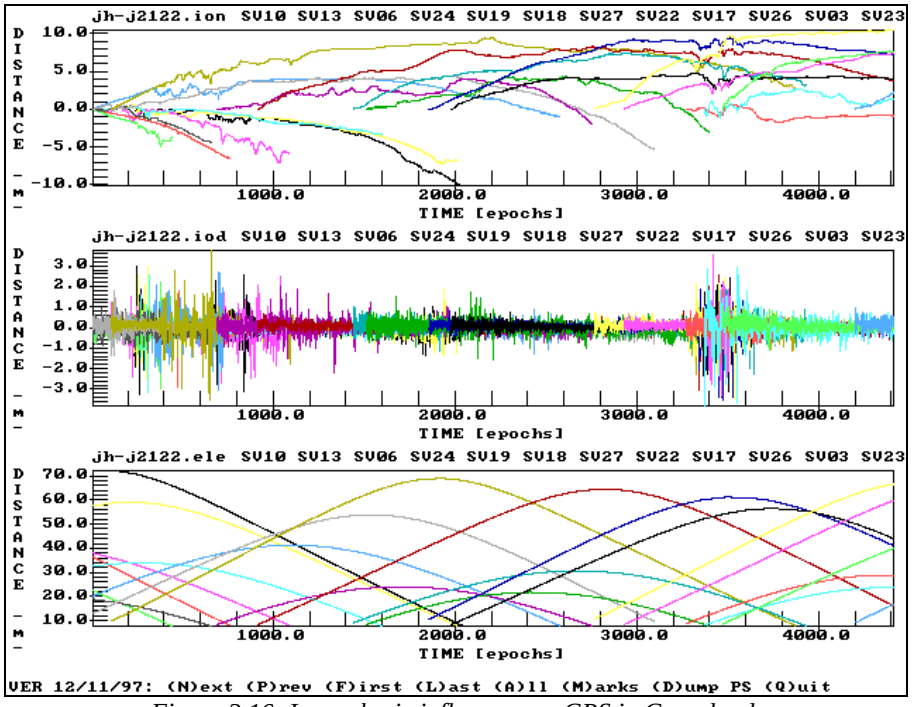


*Figure 3.16: Ionospheric influences on GPS in Greenland.*

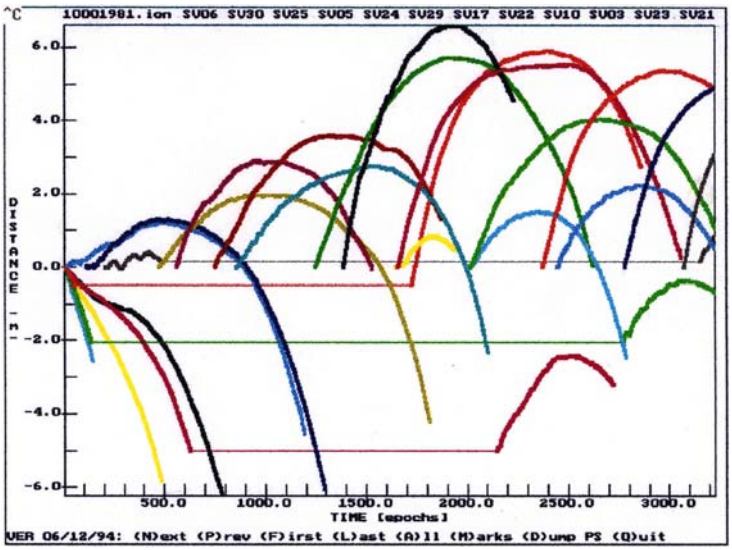


*Figure 3.17: Ionospheric influences on GPS in Stuttgart.*

*Height changes*

The results from 1999 are reduced to the date of 30th July 1999. For every campaign we had re-measured all the previous locations of all four poles in order to compare the old with the new height measurements. The point names include the number, position and measuring year. For example 120/A-94/99 means the point number 120/A at position in the year 1994, measured again in the year 1999. The location coordinates correspond to the old position 1994; the height is measured in 1999. The ellipsoidal height measurements were reduced to the ice horizon, for all the measured points between 1991 and 1999, and for all the poles (Fig. 3.18).

The figures sometimes show bigger differences from a general trend. In order to give a significant answer about height changes in the entire test fields, two causes have to be studies: Homogeneity in all the four points and homogeneity in time (measuring year).

*Homogeneity between all the four points.*

The height change is plotted as a function of position, dH = F(x, y). Even if there is a time (year) dependent height change, it would affect all points (positions x, y) likewise. This test will show problems in individual measuring related procedures, such as reduction from snow to ice horizon, reconstruction of the old point situation, accidental or even cross errors in the GPS-computation, especially problems in ambiguity resolution, multipath and ionospheric influences. The test is not able to detect common errors in the baseline JAV-Camp.

This test will show problems in individual measuring related procedures, such as reduction from snow to ice horizon, reconstruction of the old point situation, accidental or even cross errors in the GPS-computation, especially problems in ambiguity resolution, multipath and ionospheric influences. The test is not able to detect common errors in the baseline JAV-Camp.

In Figure 3.19 the height changes as shown for the years 91, 94, 95 and 96 in relation to their first height, which are re-measured in all the following campaigns. The polygons have different length, because the places 91 were re-measured 94, 95, 96 and 99, but places 96 only in 99.

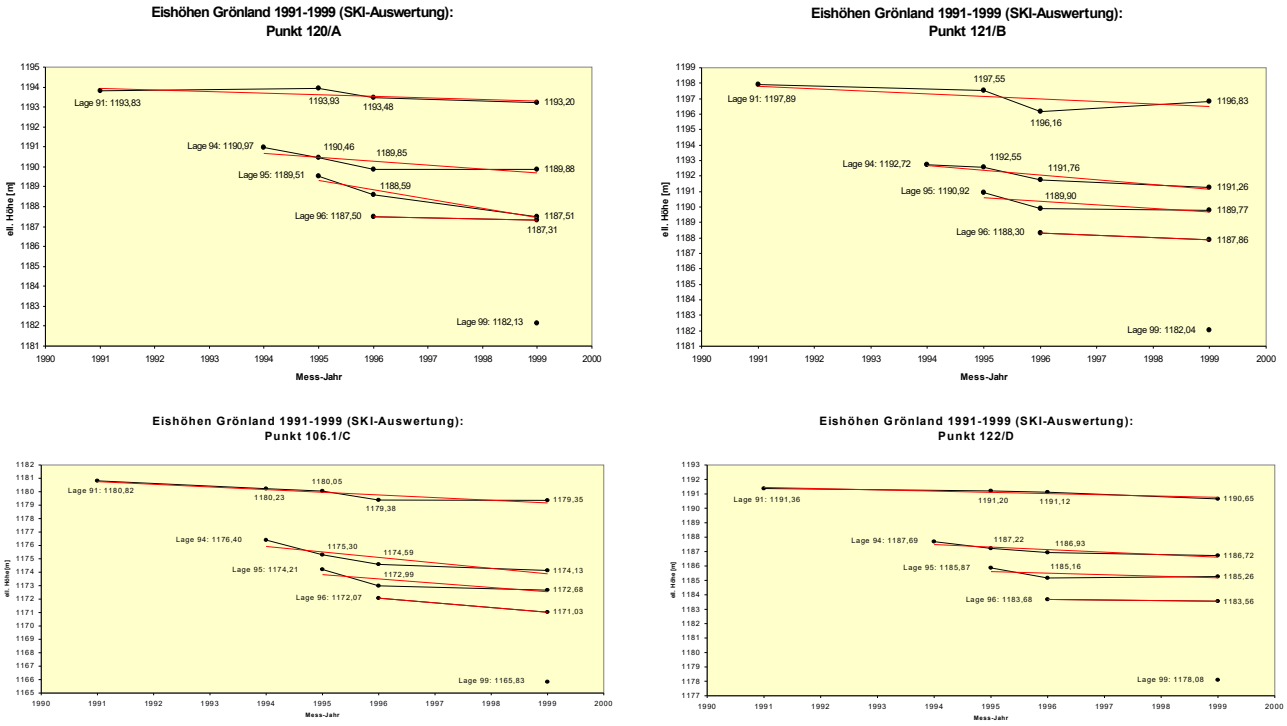

*Figure 3.18: Elevation of ice surface at all 4 sticks, situated in 1991 - 1999*

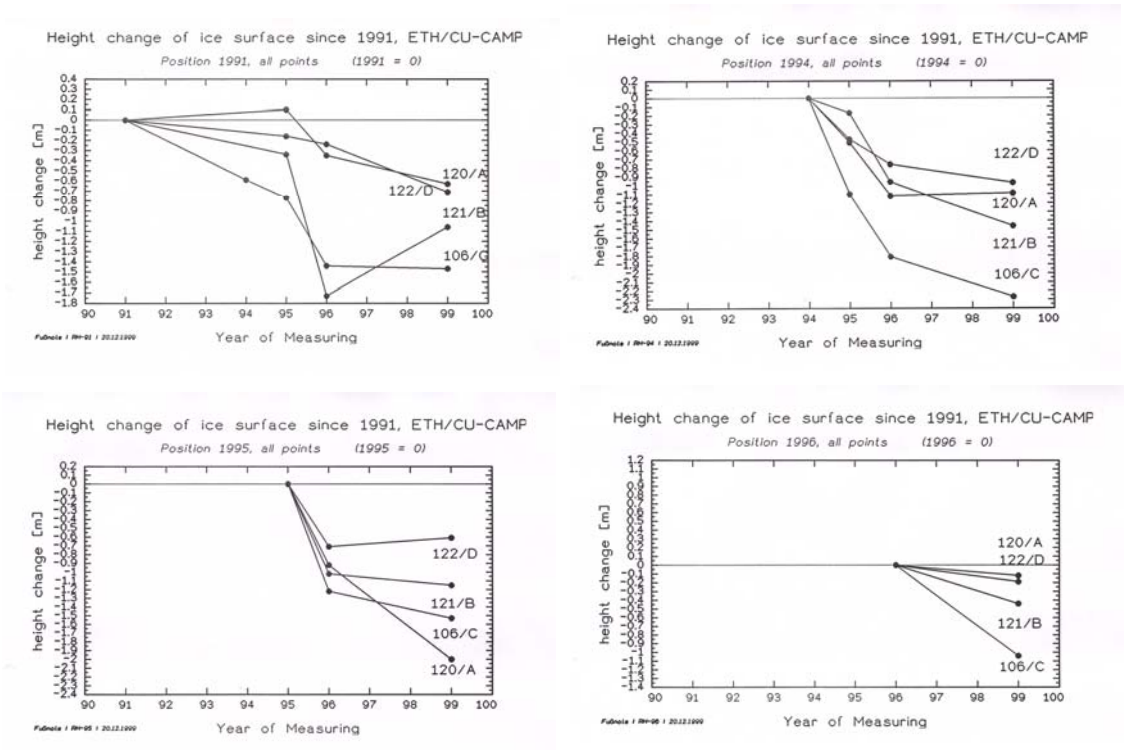


*Figure 3.19: Height changes (1991 to 1996) of all points A, B, C, D re-measured in 1991, 94, 95, 96, 99.*

We should expect the same polygons for every situation, but we observe large deviations:

1. 120/A-95/99 deviation of about 1 m, probably caused by problems in GPS ambiguity resolution.
2. 121/B-91/96 deviation of about 1 m, probably caused by problems in GPS ambiguity resolution.
3. Point 106/C is often measured too high, if it is situated near the camp, which occur when situation and measuring year are identical. This can be seen in 106/C-94/94 and 96/96, and also in 91/91. The cause is a disturbed surface around the camp by snowdrift and whirl. We find a bigger accumulation near the camp resulting in an elevation that is about 0,7 meters higher than in the undisturbed area.

Assuming a time linear behavior, we calculate the height change from all measurements (computation by SKI) as an adjusted straight line between 1991 and 1999 of -0,21 ± 0,04 m/a. The corresponding computation by the Bernese software gives -0,23 ± 0,034 m/a, so we find on average a significant height decrease of -0,22 meter per year.

*Homogeneity between different time epochs*

As we have shown in a previous report published in 1997 (campaign 1996), the height changes are varying substantially during different years. Completed with the results from 1999 we obtain an average height change of

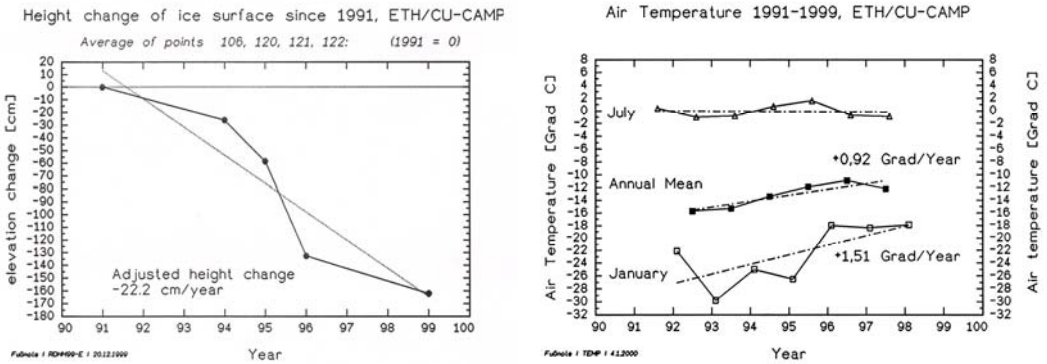

the whole test area (Fig. 3.20). We again find a continuos trend, but with variations between different time periods: Between 1991 and 1994 the yearly height change is -0,09 m/a, between 1994 and 1995 -0,32 m/a, between 1995 and 1996 -0,74 m/a and between 1996 and 1999 again only -0,08 m/a. The whole period 1991 to 1999 gives the previously quoted value of -0,215 m/a.

*Figure 3.20: Average surface height change at the ETH/CU camp (also called Swiss Camp) on the left, and air temperature data from the automatic weather station at the camp for the years 1991-1999 on the right.*

It is interesting to compare the height changes with air temperature variations, which are known from 1991 until middle of the year 1998 (K. Steffen, personal communication 1999). The mean January temperatures, the mean July temperatures and the annual mean temperatures are shown in Figure 3.20.

The adjusted straight line of July temperatures shows an almost constant temperature (with yearly variations). The January temperatures have a clear positive trend +1,5 °C/a. Due to these warmer winter temperatures the adjusted mean annual temperature indicates a substantial increasing of +0,92 °C/a. Comparing the linear trends we can state that the mean annual height decrease of -0,22 m/a is evidently corresponding to the temperature increasing of +0,9 °C/a.

We now study the variations of heights and temperatures around the linear trends in detail. It is not important which one of the temperatures we use, because they all have the same tendency in deviations from the linear trend in the same periods. The comparison shown in Figure 3.21 is performed with the most reliable mean annual temperature.

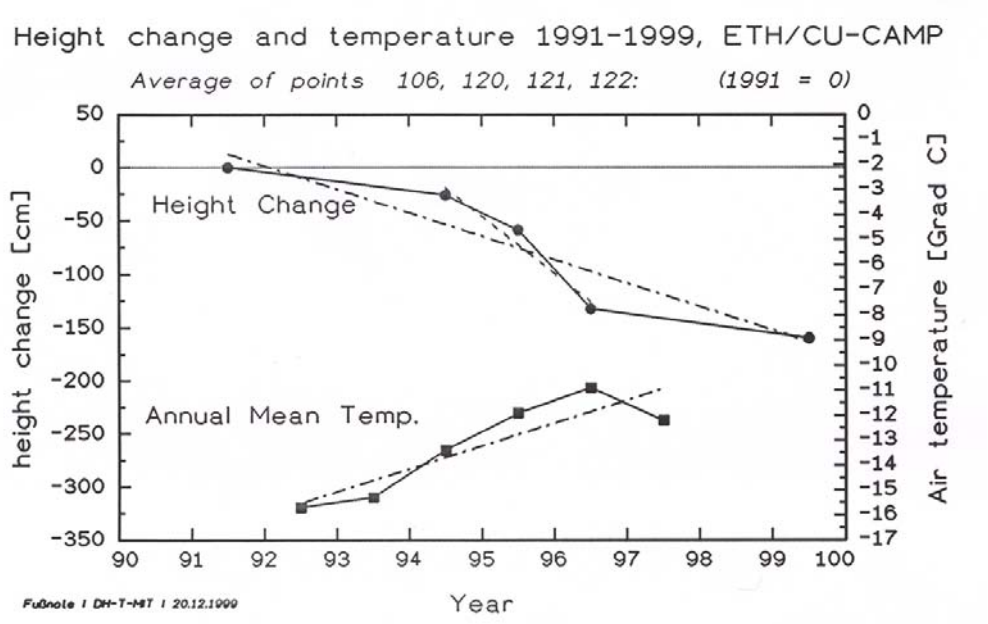


*Figure 3.21: Average surface height change and mean annual air temperature for the Swiss Camp (1991-1999).*

In spite of the fact that due to different time intervals no cross correlation can be calculated, we clearly see, that a temperature increasing is corresponding to a height decreasing in the period 95-96. In the periods 91-94 and 96-99 the subaverage temperature increasing is corresponding to the subaverage height decreasing.

So we can conclude that the height of the inland ice at the ETH/CU-camp is surprisingly fast to react to climatic changes. Both the long-termed trend and the short periodic temperature variations are influencing ice thickness.

### *3.5.2 Topographical survey of the ice surface: Comparison to 1995*

The topographical survey was performed by trigonometric leveling and Real-Time-GPSl. Due to lack of time we could only measure a rough grid with 100-200 m resolution. In order to reduce the heights from snow to ice surface we measured the thickness of the snow layer in the snow pits (average only 0.20 m).

Figure 3.22 depicts the surveying area as shown by a map (Fig. 3.22: elevation isolines). The local coordinate system has its origin in point 106/C-99/99 nearby the camp. It is compared to the survey of 1995, because in 1995 we measured approximately the same area. The difference in volume over the 1995-1999 period is –827,374 $m^3$ above an area of 820,880 $m^2$, which corresponds to a decrease in thickness of -1,01 meters in 51 month; or –0.24 m/a. From the difference model (Fig. 3.23) we see some local variations, especially around the camp, where the snow accumulation is always substantially disturbed.

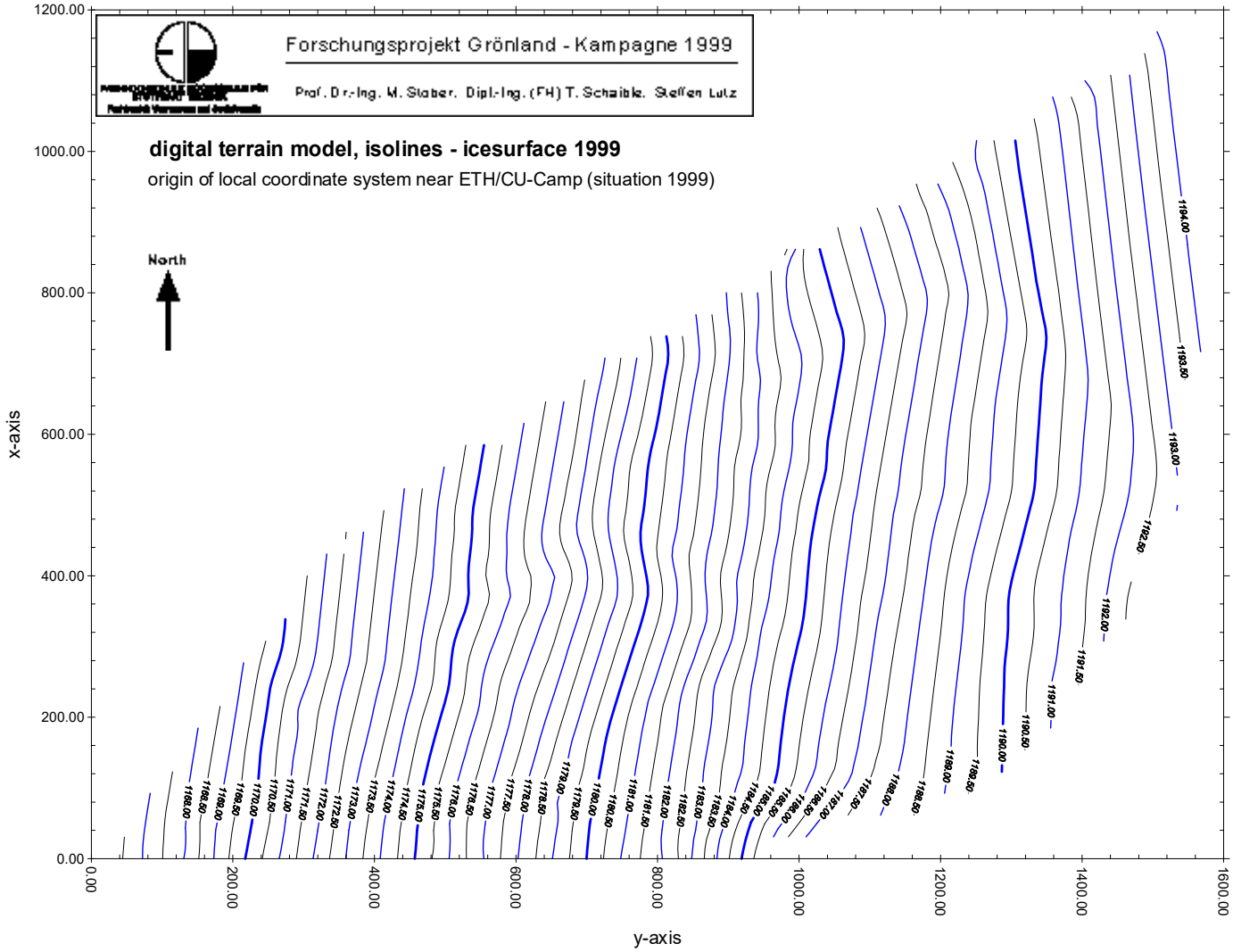


*Figure 3.22: Digital terrain model (isolines), ice surface 1999*

*Ice flow vector*

Ice flow velocity and direction are well known from the previous campaigns 1991 until 1996. Nevertheless it is still interesting to see whether they will change under other climatic conditions. Table 3.6 shows a summary of the new values 1996-1999 compared with those of the other epochs.

*Table 3.6: Ice velocity at the Swiss Camp for the years 1991-1999.*

| Period | Ice flow velocity [m/day] | Azimuth of flow [gon] |
|---|---|---|
| 1991-1994 | 0.313 ± 0.001 | 259.60 ± 0.27 |
| 1994-1995 | 0.319 ± 0.001 | 260.44 ± 0.12 |
| 1995-1996 | 0.313 ± 0.001 | 260.25 ± 0.12 |
| 1996-1999 | 0.320 ± 0.001 | 260.68 ± 0.12 |
| Weighted Mean | 0.316 ± 0.002 | 260.40 |

There are some small discrepancies, especially at the azimuth. These are not significant as the standard deviations are only calculated from inner accuracy, which does not include absolute influences like less precise positioning in 1991. So we have to state a constant flow vector over the whole period 1991 to 1999.

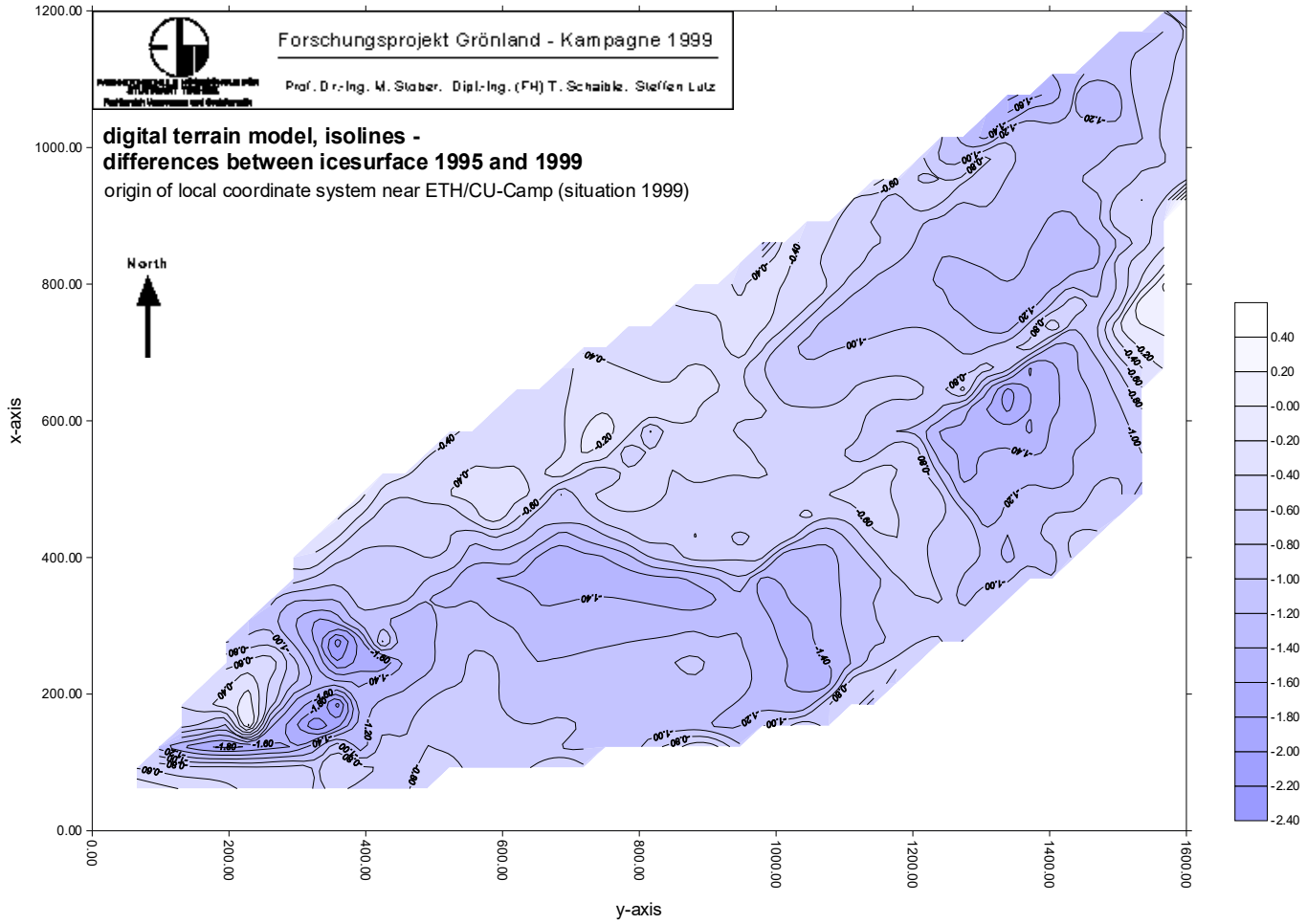


*Figure 3.23: Digital terrain model (isolines), difference between ice surfaces 1999 and 1995.*

*Deformation and strain*

The deformation figure, consisting in the 4 points A,B,C,D (triangle with central point) is distorted by stresses, which induce deformation and strain. Deformations, strain and strain rates are essential parameters for mass balance studies. In contrast to previous campaigns we now calculate the principal axis of strain and strain rates.

As basis we use the networks in different epochs, which are given in a common local coordinate system. In case of deformation by homogeneous stress between two epochs the two nets can be transformed on each other by an affine coordinate transformation.

The linear transformation equations are given by:

$X' = a_0 + a_1*X + a_2*Y$
$Y' = b_0 + b_1*X + b_2*Y$

With X ,Y as a starting system with original shape (epoch 1) and X',Y' as an end system after deformation (epoch 2). In case of more than 3 points, the six unknown parameters $a_i$, $b_i$ are to be calculated from a least squares adjustment.

From the parameters $a_i$, $b_i$ we obtain by simple relations (Welsch, 1982) the strain rates in direction of coordinate axis (X,Y):

$e_{xx}$ = Strain rate from normal stress in x-axis
$e_{yy}$ = Strain rate from normal stress in y-axis
$e_{xy}$ = Strain rate from shear stress

and direction (azimuth) $\Phi$ and amounts $e_1$, $e_2$ of extreme horizontal strain rates (principal axis of the so called strain ellipse). Strain is defined as relative deformation ($\Delta L/L$), dimension ppm; strain rates are time derivatives of strain, dimension ppm/a. Assuming incompressibility of ice, together with $e_3$ as strain rate in vertical direction, the following condition exists:

$e_1 + e_2 + e_3 = 0$,
and, therefore:

$e_3 = -(e_1 + e_2)$ [ppm/a].

If we know the ice thickness H, which is about 800 m in the camp area, we are able to calculate the thickness change $\Delta H$ from:

$\Delta H = e_3 * H$.

The strain was calculated between the campaigns in 94, 95, 96 and 99. As an example the results from triangle ABC between 1994 and 1999 (the longest period with precise positioning) are shown in the following table.

*Table 3.7: Strain rates of triangle ABC, 1994 to 1999*

| Epoches | | Azimuth [gon] principal axis | | Strain rates [ppm/a] | | | ΔH/a |
|---|---|---|---|---|---|---|---|
| 1 | 2 | $e_1$ | $e_2$ | $e_1$ | $e_2$ | $e_3$ | [m/a] |
| 94 → 99 | | 21.8 | 121.8 | +1115 | -815 | -300 | -0.24 |

The height change calculated from the incompressibility condition is –0.24 m/a, which is surprisingly good agreeing with the results from GPS-measurements (-0.22 m/a).

### *3.5.3 Conclusions and outlook*

The height change (decreasing) of about –0.22 m/a is somehow related with an increasing air temperature of about +0.9 °C/a. Even yearly variations can be explained by temperature deviations from the long-termed trend. Therefore we can make some general conclusions.

*Equilibrium line*

In West Greenland the equilibrium line is situated in an elevation between 1150 and 1200 meter above sea level (Reeh, 1991). Our research area is located at 1150 m and therefore be representative for the equilibrium line altitude. In a stable ice body we would not expect any height changes near the equilibrium line. However, we found decreasing heights of –0.22 m per year. Perhaps the Reeh (1991) modeling was not successful due to

lack of data, or because of insufficient boundary conditions. It is also possible that the model assumptions were correct, but a change in climate occurred. Higher temperatures will increase the melting at lower elevations, and at higher elevations the accumulation rate might be increasing due to additional precipitation. Consequently, the ablation area will increase and the accumulation area will decrease, but the total mass of the ice sheet may increase due to additional precipitation (accumulation area is much larger than ablation area).

Indications for a displacement of ice masses have been reported based on satellite data (Krabill, 1999; Rignot, 1997), with thickening in the central parts, and a thinning in lower parts, particularly in the southeast of Greenland (-1 m/a). Satellite and aircraft derived data (microwave or laser altimetry, respectively) need verification, and our results, which are determined by terrestrial and independent methods may be useful as control areas for remote sensing methods. It is interesting, that Krabill et al. (1999) also found decreasing heights at the ETH/CU-camp in the same magnitude of –0.2 to –0.3 m/a, indicating that ground-based GPS-data and satellite data show good agreement.

*Influences on Jakobshavn Glacier*

The Jakobshavn Glacier is one of the most productive glaciers in the world in terms of iceberg calving. The height lowering of the inland ice (-0.22 m/a) might diminish the influx of ice masses to the glacier. It could be compensated by a faster flow velocity of the glacier, as stated by Krabill et at. (1999) for other parts of Greenland. We don't have the most recent ice velocity values for the glacier tongue, but our measurements at the ETH/CU-Camp suggest that the ice velocity has not changed in recent years.

*Continuation of the EGIG-profile towards the western margin*

The geodetic investigations of the International Glaciological Greenland-Expedition (EGIG) 1959, 1968 and 1990-1992 had found an increase in height of +0.1 to +0.2 m/a for the inner part of Greenland ice sheet during the period 1959-68, and a decreasing in surface height of –0.2 m/a between 1968-92 (Möller et al. 1996). Results are missing for the western margin of the ice sheet, up to an elevation of 1700 m (about 80 km).

The ETH/CU-Camp is situated at 1150 m elevation, and may cover this gap at least as a single point. The surface height change of –0.2 m/a is in good agreement with the results from the EGIG line. However, we have to consider that both results do not refer to the same time period. Determining height changes is only possible by long-termed observations. Satellite and terrestrial methods have to be compared to and verify each other.

# 4. PROPOSED RESEARCH 2000 AND BEYOND

## *4.1 Greenland ice sheet climatology and surface energy balance*

The turbulent energy fluxes will be derived using the aerodynamic method (bulk transfer) and the Monin-Obukhov similarity theory for the flux-gradient relations of non-neutral surface layer conditions (Garrett, 1992). As input parameters, the AWS temperature, humidity and wind speed profile data will be used. For the ground heat flux, the AWS snow temperature profile will be used. These fluxes will be compared against the net radiation, which is measured as one of the AWS parameters. In the ablation and wet-snow region of the ice sheet (JAR, Swiss Camp, Dye-2, Dye-3) the residual of the surface energy balance equals the energy used for melting ice or snow during the summer months, which can be validated with the acoustic snow depth sensors. The results of energy balance models are most sensitive to the parameterization of the turbulent heat fluxes (Van de Wal and Oerlemans, 1994). Reducing the uncertainties in the parameterization of the turbulent heat fluxes with field measurements at the different AWS locations will improve the results. Therefore, the surface energy balance will be calculated and parameterized for each AWS site, and be used as a site specific information (i.e., altitude, latitude, slope, or distance from ice margin ) for the energy balance model. We will use an energy balance model as proposed by Van de Wal and Oerlemans (1994), with improved parameterizations for the turbulent (sensible and latent) and radiative fluxes.

The emphasis of this proposed work is on the climate system model interface, combining the atmosphere and the cryosphere component over the Greenland ice sheet. The objective of this study is to model the surface energy balance based on the atmospheric and cryospheric interactions, and to replicate the present precipitation and accumulation pattern on the ice sheet. Further, we anticipate to model sublimation/deposition rates based on energy balance models and GC-Net data input. The link between climate and ice sheet is forged through the net surface mass balance. Numerous studies have been performed to investigate the energy balance at single points in Greenland (Ambach, 1963; Ohmura et al., 1994; Steffen, 1995), but to date only a few attempts have been made to investigate the energy balance for the entire ice sheet. Van de Wal and Oerlemans (1994) proposed a model for the entire Greenland ice sheet, but the model reliability was not examined. Surface energy balance sensitivity tests in the past have shown (Greuell and Oerlemans, 1986), that ablation is very sensitive to variations in atmospheric temperature, humidity, cloudiness and wind speed. The ablation on the Greenland ice sheet appears to be quite sensitive to temperature change according to Van de Wal and Oerlemans, (1994). They found a 1K-temperature rise produces a 34% increase in the mean ablation. We propose to test the energy balance model sensitivity to the variation of input parameters by using data from the present and proposed AWS network. The proposed AWS network is essential for the assessment of the Greenland surface climatology as only five air temperature records exist (excluding the here discussed AWS network) that cover an entire annual cycle for interior locations of the ice sheet, with the record length between one and three years [Reeh, 1989].

The results from our surface energy balance will be compared with NCEP, ECMWF and GISS99 model outputs, and the sensitivity of these models to subscale parameter variability will be investigated. Since we are not experts in GCM modeling, we will collaborate with other groups (e.g., Ohio State University, Dr. D. Bromwich; Canadian Center for Climate Modeling and Analysis, Dr. G. Flato).

Satellite derived surface parameters such as snow facies (dry snow, wet snow, bare ice), surface albedo, surface temperature, and cloudiness are additional input parameters for the energy balance model. We will use passive microwave satellite data (SSM/I) and scatterometer data (QuikSCAT ) to derive the wet snow extent, MODIS and AVHRR for surface temperature and albedo retrieval, and possibly GLAS lidar data for cloud classification in the energy balance modeling boundary conditions.

Furthermore, the surface topography with scale length of several kilometers plays an important role for the spatial variability of accumulation, the mass transfer, and the surface energy balance. Due to the compression of air over these undulations (wavelength of 5 km with 30-50 m amplitude), the turbulent energy fluxes are strongly modified, and consequently the sublimation rates. Using AVHRR and MODIS photoclinometry, in combination with laser/GPS aircraft data, we will parameterize the surface of the Greenland ice sheet. The knowledge of this surface roughness is essential for the spatial surface energy balance modeling. We anticipate collaboration

with Dr. Waleed Abdalati, NASA/GSFC on the termination of ice sheet topography. In addition, we will measure the spatial variability of the accumulation with ground penetrating radar, and use the results in our models.

### *4.2 Anticipated Results*

*Greenland Surface Climatology*

Data processing and analysis:

- develop data cleaning and interpolation programs for AWS data sets
- process and calibrate all AWS parameters
- calculate surface energy balance (turbulent, conductive and radiative fluxes) for each AWS location and parameterize site specific flux parameters
- develop interpolation schemes to generate surface climatology maps with AWS data and coastal meteorological data sets
- generate gridded climatological fields for energy balance model input
- develop cloud classification algorithm based on AWS radiation data and analyze cloud climatology fields for Greenland. Provide year-round cloud statistics for future satellite laser missions (i.e., GLAS).

Data and technical information will be accessible through:

- the PARCA homepage http://cires.colorado.edu/steffen/
- anonymous ftp account on seaice.colorado.edu in directory /pub/parca/

*Energy Balance Model*

Satellite data input, model parameterization, model sensitivity and output:

- parameterize satellite derived surface fields such as albedo, surface temperature, and clouds for energy balance model input
- develop energy balance model based on AWS site specific flux parameterization and satellite derived surface fields
- analyze model sensitivity to input parameters and determine model response to external forcing
- validate model output with in situ energy flux measurements from the Swiss camp (eddy correlation measurements made between 1990 and 1999)
- analyze seasonal and interannual variations of the surface energy balance for the entire Greenland ice sheet based on three years data acquisition and spatial interpolation
- identify areas of largest sensitivity to surface energy balance changes due to climate perturbation
- compare energy balance model results with GCM model out such as NCEP, ECMWF, and GISS99

### *4.2 Time Table*

***Year 1:***

Install an AWS in the lower ablation region near Sonderstromfjord on the west coast, and near Kulusuk on the east coast of Greenland. Service AWS at Dye-2, Saddle, KULU, NASA-SE, Crawford Point1, Crawford Point 2, JAR1 and JAR2. Furthermore, we plan to re-visit Swiss Camp for 3 weeks to continue eddy correlation turbulent measurements, collect high-resolution GPS measurements of ice motion, and to make ground-penetrating radar profile measurements between the Swiss Camp and Crawford Point ((150 km). The spatial variability of the energy exchanges are important for flux parameterization and ultimately energy balance modeling. The collected AWS data throughout 2000 will be processed and analyzed, and made available for the PARCA group on the homepage (http://cires.colorado.edu/steffen/)

***Year 2:***

Service AWS network where needed. Re-visit the Swiss camp for period of 3-4 weeks. Finish analysis of sublimation estimates of the Greenland ice sheet (Ph.D. thesis Jason Box) and publish results. Finish parameteriza-

tion of energy fluxes and transfer coefficients using AWS network data and eddy correlation measurements from the Swiss Camp. Provide ground-truth data for NASA's ICESAT mission (launch date 2001).

***Year 3:***
Service AWS network where needed. Re-visit the Swiss camp for period of 2-3 weeks. Finish surface energy balance modeling effort, and compare results with NCEP, ECMWF and GISS99 model output. Provide ground-truth data for NASA's ICESAT mission (launch date 2001).

***Year 4:***
Service current AWS network where needed. Re-visit the Swiss camp for period of 4 weeks. The main objective for that year will be on the sensibility study of the surface energy balance model runs for the Greenland ice sheet using present past and predicted surface climatologies, which will be produced earlier in the project from AWS and satellite data. Provide ground-truth data for NASA's ICESAT mission (launch date 2001).

## 5. REFERENCES


Ambach, W., Untersuchungen zum Energieumsatz in der Ablationszone des grönländischen Inlandeises. *Medd. Groenl*., **174(4),** 1966.

Anderson, P. S., A method for rescaling humidity sensors at temperatures well below freezing, *J. Atmos. Oceanic Tech*., **11(11),** 1388-1391, 1994.

Anderson, P. S., Reply to Comments on "A method for rescaling humidity sensors at temperatures well below freezing", *J. Atmos. Oceanic Tech*., **13(4),** 913-914, 1996.

Brutsaert, W., Evaporation into the Atmosphere: Theory, History, and Applications, Kluwer Academic Pub., **299**, 1982.

Deardorff, J.W., Dependence of air-sea transfer coefficients on bulk stability. *J, Geophys. Res*., **73**, 2549-2557, 1968.

Dyer, A. J., A review of flux-profile relationships, *Boundary Layer Met*., **7**, 363-372, 1974.

Greuell, W., and J. Oerlemans, Sensitivity studies with a mass blaance model including temperature profile calculations inside the glacier*, Z. Gletscherkunde und Glazialgeologie*, **22**, 101-124, 1986.

Hay, J.E. and B.B. Fitzharris, The synoptic climatology of ablation on a New Zealand Glacier. *J Climatol*., **8**, 201-215, 1988.

Ishikawa, N., I.F. Owens, and A.P. Sturman, Heat balance characteristics during fine periods on the lower parts of the Franz Josef Glacier, South Westland, New Zealand. *International Journal of Climatology*, **12**, 397-410, 1992.

Kelliher, F.M., B.M.M. Kostner,, D.Y. Hollinger, J.N. Byers, J.E. Hunt, T.M. McSeveny, R. Meserth, P.L. Weir, and E.D. Schulze, Evaporation, xylem sap flow, and tree transpiration in a New Zealand broad-leaved forest. *Agric. For. Meteorol*., **62**, 53-73, 1997.

Krabill, W. et al, Rapid thinning of parts of the southern Greenland Ice Sheet, *Science*, **283**, 1522-1524, 1999.

Lettau, H., Wind and temperature profile prediction for diabatic surface layers including strong inversion cases, *Boundary Layer Met*., **17**, 443-464, 1979.

Makkonen, L., Comments on "A method for rescaling humidity sensors at temperatures well below freezing", *J. Atmos. Oceanic Tech*., **13(4),** 911-912, 1996.

Hansen, J., M. Sato, R. Ruedy, A. Lacis, and 39 co-authors, Forcings and chaos in interannual to decadal climate change*. J. Geophys. Res*., **102**, 25679-25720, 1997.

Möller D., et al., Die Weiterführung der geodätischen Arbeiten der Internationalen Glaziologischen Grönland Expedition (EGIG) durch das Institut für Vermessungskunde der TU Braunschweig. Deutsche Geod. Kommission, Reihe B, Nr. **303**, München 1996.

Moore, R.D., and I.F. Owens, Controls on advective snowmelt in a maritime alpine basin. *J Clim. Appl. Meteorol*., **23**, 135-141, 1984.

Munro, D.S., Surface roughness and bulk heat transfer on a glacier: comparison with eddy correlation. *Journal of Glaciology*, **35**, 343-348, 1989.

Ohmura A., and 6 others, Energy balance of the Greenland ice sheet by observation and model computation, *IAHS Publ*., **223,** 85-94, 1994.

Oke, T.R., *Boundary Layer Climates 2nd ed*. Menthuen, London, pp.435, 1987.

Reeh, N., Parameterization of melt rate and surface temperature on the Greenland ice sheet. *Polarforschung*, **59(3),** 113-128, 1989.

Price, A.G., and T. Dunne, Energy balance computations of snowmelt in a subarctic area. *Water Resour. Res*., **12**, 686-694, 1976.

Reeh, N., Parameterization of melt rate and surface temperature on the Greenland Ice Sheet, *Polarforschung*, **59(3)**, 113-128, 1989.

Rignot, E.J. et al., North and northeast Greenland ice discharge from satellite Radar interferometry, *Science*, **276**, 934-937, 1997.

Stearns, C.R., and G.A. Weidner, Sensible and latent heat flux estimates in Antarctica. *Antarctic meteorology and climatology*, **61**, 109-138, 1993.

Steffen, K., Surface energy exchange at the equilibrium line on the Greenland ice sheet during onset of melt. *Annals of Glaciology*, **21**, 13-18, 1985.

Stull, R.B., *An introduction to Boundary Layer Meteorology*. Kluwer Publishers, Dordretcht, pp. 666. 1988.

Tanner, B.D., and J.P. Green, Measurement of sensible and vapor fluxes using eddy correlation methods. Final report prepared for the U.S. Army Dugway Proving Grounds, Dugway, Utah, February 27, 1989.

Van de Wal, R.S.W., and W. J. Oerlemans, An energy balance model for the Greenland ice sheet, *Global and Planet. Change*, **9**, 115-131, 1994.

Webb, E.K., Pearman, G.I., and Leuning, R., Correction of flux measurements for density effects due to heat and water vapor transfer. *Quart. J. Roy. Meteorol. Soc*., **106**, 85-100, 1980.

Welsch W., Description of homogeneous horizontal strains and some remarks to their analysis, *Deutsche Geod. Kommission*, Reihe B, Nr. **258/V**, 188-205, 1982.

## 6. PUBLICATIONS SUPPORTED FROM THIS GRANT

Abdalati, W., and K. Steffen, Snowmelt on the Greenland ice sheet as derived from passive microwave satellite data, J. Climate, 10(2), 165-175, 1997.

Abdalati, W., and K. Steffen, The apparent effects of the Mt. Pinatubo eruption on the Greenland ice sheet melt extent, Geophys. Res. Lett., 24(14), 1795-1797, 1997.

Abdalati, W., and K. Steffen, Accumulation and hoar effects on microwave emission on the Greenland ice sheet dry snow zones, J. Glaciology, 44(148), 523-531, 1998.

Anklin, M., R.C. Bales. E. Mosley-Thompson, and K. Steffen, Annual accumulation at two sites in northwestern Greenland during recent centuries, J. Geophysical Research, 103(D22), 28775-28,783, 1998.

Box, J., and K. Steffen, An empirically based model for estimating blowing snow mass fluxes for the Greenland Ice Sheet, 5th Int. Conf. Polar Met. and Oceanogr., Dallas Jan 10-15 1999, 79 Annual Amer. Met. Soc. General Meeting, paper 12.7, 1999.

Serreze, M., J. Key, J. Box, J. Maslanik, and K. Steffen, A new monthly climatology of global radiation for the Arctic and comparison with NCEP-NCAR reanalysis and ISCCP-C2 field, J. Climate, 11, 121-136, 1998.

Steffen, K., Effect of solar zenith angle on snow aniosotropic reflectance, IRS '96: Current Problems in Atmospheric Radiation, Smith and Stamnes (Eds), Deepak Publishing, 41-44, 1997.

Steffen, K., W. Abdalati, and I. Seherjal, Faceted crystal formation on NE-Greenland low accumulation region, J. Glaciology, 45(149), 63-68, 1999..

Steffen, K., and J. Box, Recent climate variability of the Greenland ice sheet: first results from the Greenland climate network, 5th Int. Conf. Polar Met. and Oceanogr., Dallas Jan 10-15 1999, 79 Annual Amer. Met. Soc. General Meeting, paper 4.6, 1999.

Stroeve, J., M. Haefliger, and K. Steffen, Surface temperature fro ERS-1 ATSR infrared thermal satellite data in Polar regions, J. Appl. Meteorol., 35(8), 1231-1239, 1996.

Stroeve, J., A. Nolin, and K. Steffen, Comparison of AVHRR-derived and in situ surface albedo over the Greenland ice sheet, Remote Sens. Environ., 62, 262-276, 1997.

Stroeve, J., and K. Steffen, Variability of AVHRR-derived clear-sky surface temperature over the Greenland ice sheet, J. Appl. Meteorol., 37, 23-31, 1998.

Stroeve, J., and A. Nolin, The changing albedo of the Greenland ice sheet: implications for climate modeling, Ann. of Glaciol. 25, 51-57, 1997.

Steffen, K., J. Box, and N. Cullen, Monthly mean climatology for Greenland's automatic weather station, submitted to JGR special PARCA issue.

Steffen, K., N. Cullen, and J. Box, Sensible and latent heat flux estimates and radiation balance for the Greenland ice sheet, submitted to JGR special PARCA issue.

Box, J., K. Steffen, N. Cullen, Evaporative mass transfer from the surface of the Greenland ice sheet, submitted to JGR special PARCA issue

# 7. PROPOSED FIELD WORK 2000

## *7.1 AWS Maintenance and Swiss Camp Experiments*

During the new field season we propose to service up to 11 automatic weather stations. For six stations the maintenance will be crucial for the overall performance of the GC-Net (high priority).

| **Site** | **Description** | **Twin Otter Otter Flt Hours*** | **Priori-ty** | **Time Needed On Site **** |
|---|---|---|---|---|
| Swiss Camp | • Maintenance<br>• Add IR sensor | 3.5 | High | 1-3 days |
| DYE-2 | • Mast extension<br>• Maintenance | 1.5 or C-130 | High | 1-3 days |
| NASA-SE | • Mast extension<br>• Maintenance<br>• Add transmitter | 3.5 | High | 1-3 days |
| KULU | • Reconnaisance<br>• Mast extension.<br>• Maintenance | 1.5 heli<br>+ commercial flt. to SE | High | 1-2 days |
| CP-2 | • Mast extension<br>• Maintenance | Skidoo:<br>incl. W/ Swiss Camp | High | 1-2 days |
| Saddle | • Replace transmitter | 1 hour if combined w/NASA-SE flight. | High | 1-1.5 hour pit stop |
| NGRIP | • Mast extension<br>• Maintenance | C-130*** | Medium | 1-3 days |
| NASA-E | • Mast extension<br>• Maintenance | 6 incl. w/Tunu-N | Medium | 1-3 days |
| JAR-2 | • Mast extension<br>• Maintenance | Skidoo:<br>incl. W/ Swiss Camp | Medium | 1 day |
| CP-1 | • Manitenance | Skidoo: incl. W/ Swiss Camp | Medium | 1 day |
| TUNU-N | • Mast extension<br>• Maintenance | 8#<br>20## | Medium | 1-3 days |

* - unless otherwise noted.
** - Less time on site is possible but does not allow much time for unforseen problems and rest.
*** -NGRIP transport is supported by the Danes
# - if Twin Otter is in Constable Point
## -if we have to fly from Sonderstrom Fjord